ISSN 1562 - 2703

INTERNATIONAL JOURNAL AUTOMATION AUSTRIA

Heft 2 im Jahrgang 19 (2011)

Inhalt *Seite*

SCOPE

"International Journal Automation Austria" (IJAA) publishes top quality, peer reviewed papers in all areas of automatic control concerning continuous and discrete processes and production systems.

Only original papers will be considered. No paper published previously in another journal, transaction or book will be accepted. Material published in workshops or symposia proceedings will be considered. In such a case the author is responsible for obtaining the necessary copyright releases. In all cases, the author must obtain the necessary copyright releases before preparing a submission. Papers are solicited in both theory and applications

Before preparing submissions, please visit our instructions to authors (see back cover) or web page.

International Journal Automation Austria also is the official executive authority for publications of IFAC-Beirat Österreich.

Imprint: Propagation of Automatic Control in Theory and Practice.

Frequency: Aperiodically, usually twice a year.
Publisher: IFAC-Beirat Österreich, Peter Kopacek, Alexander Weinmann
Editors in Chief: Alexander Weinmann, Peter Kopacek

Address: 1) Institut für Automatisierungs- und Regelungstechnik (E376), TU Wien,
A-1040 Wien, Gußhausstrasse 27-29, Austria
Phone: +43 1 58801 37677, FAX: +43 1 58801 37699
email: danzinger@acin.tuwien.ac.at
Homepage: http://www.acin.tuwien.ac.at/publikationen/ijaa/

2) Intelligente Handhabungs- und Robotertechnik (E325/A6), TU-Wien,
A-1040 Wien, Favoritenstrasse 9-11, Austria
email: e318@ihrt.tuwien.ac.at

Layout: Rainer Danzinger
Printing: Grafisches Zentrum an der TU Wien

Energy Efficient Model Predictive Control of a Cooling System

A. Hofer*, F. Kitanoski#

*Graz University of Technology
Institute of Automation and Control
Kopernikusgasse 24, A-8010 Graz
anton.hofer@tugraz.at

#Virtual Vehicle
Inffeldgasse 21a, A-8010 Graz

Abstract
Hybrid electrical vehicles require additional cooling for electrical drives, power electronic circuits and batteries. Usually these cooling loops are actuated electrically which offers the possibility to implement new cooling strategies. In order to enhance the fuel efficiency of the vehicle energy optimal cooling becomes important. A model predicive control scheme for the cooling problem is presented which admits energy efficient cooling. It is a characteristic feature of the proposed control scheme that it is based on simulation and optimization. Methods for improving the prediction of future values of the external inputs have been abandoned at all in order to keep the concept simple. A comparison with the global optimum solution of the cooling problem confirms the remarkable performance of the proposed control strategy.

1 Introduction

The recent development in automotive industry is dominated by the reduction of fuel consumption and CO_2 emissions of the vehicles. Hybrid electrical vehicles are regarded to gain essential progress in coping with these requirements especially for the next few years. But the realization of hybrid power train concepts also requires appropriate cooling of the electrical components such as electrical drives, power electronic circuits or batteries. Thus the cooling problem becomes more involved. Usually additional cooling loops have to be implemented in order to provide the required cooling which implies some significant differences compared to the conventional cooling concept for a combustion engine. In the latter case the pump for the coolant is usually *belt driven* by the engine and the main goal is to keep the temperature of the engine *permanently* at a prescribed value. In the first case however the pump for the coolant is *electrically driven* and the cooling must guarantee that the temperature of the object to be cooled does not exceed a *given bound*. These facts offer the possibility for introducing a concept that can

be termed *cooling on demand.* Furthermore sophisticated cooling management systems can be developed now such that the energy used for the cooling task is as low as possible.

Although the amount of energy used for cooling is small compared to the energy used for moving the vehicle a suitable cooling strategy can improve the overall fuel efficiency. A profound rating of the performance of a cooling management system from the energetic point of view requires the knowledge of the minimum energy required for a certain cooling task. For this purpose a method for computing the energy optimal feed forward control of a cooling system has been presented in *Kitanoski, F., and Hofer, A.,2010b*. Based on these results a model predictive control (MPC) for the cooling problem is developed in this paper. Generally MPC (also termed receding horizon control) is regarded as a powerful control strategy in the presence of input constraints and/or state constraints (see e.g. *Maciejowski, J.M.,2002* and *Camacho, E.F., and Bordons, C., 1999*). Originally it was applicable to systems with slow dynamics only but due to the enhanced computational power of actual hardware and better software support (see e.g. *Mattingley, J., et al., 2010*) the scope for MPC implementations has been increased drastically.

The performance of any MPC scheme is essentially influenced by assumptions about the future behavior of the external input signals. In the present application various sources to improve the knowledge about the future driving requirements and conditions might be available e.g. from GPS data. But one should keep in mind that the thermal load produced by the object to be cooled is mainly determined by the energy management system of the hybrid electrical vehicle. This fact makes the forecast problem for the cooling task more complicated. Therefore the prediction problem is left aside in this contribution which has the beneficial effect that the resulting MPC strategy becomes more simple. Simulations of the closed loop control system reveal that energy efficient cooling can be obtained without any sophisticated prediction techniques.

2 Mathematical Model of the Cooling System

For the presentation of the proposed control method a cooling system for an electrical drive in a hybrid electrical vehicle is considered (see Fig. 1). It consists of an electrically driven pump, which forces the coolant mass flow $\dot{m}_W$ through the cooling loop. The cooling of the fluid is provided by a heat exchanger, where the air mass flow $\dot{m}_A$ can be influenced by an electrically actuated fan.

In order to derive a simple mathematical model five *lumped* masses are introduced: M_M denotes the mass of the electrical drive, M_{W1} is the mass of the coolant in the pipe from the electrical drive to the heat exchanger, M_{W2} is the mass of the coolant from the heat exchanger to the electrical drive, M_S denotes the mass of the mechanical structure of the heat exchanger and M_A is the mass of the air in the heat exchanger. The temperatures of these masses are denoted by $T_M, T_{W1}, T_{W2}, T_S, T_A$. The thermal behavior of the system is mainly determined by the *adjustable* rotational speeds n_P and n_F of the pump and the fan respectively and by the heat rate $\dot{Q}_E$ produced by the operation of the electrical drive. Furthermore the cooling effect of the heat exchanger is also influenced by the environmental temperature T_E and the velocity v of the vehicle.

Assuming that the heat capacity, the density and the viscosity of the coolant fluid are constant and neglecting the heat transfer between the pipes and the environment the following

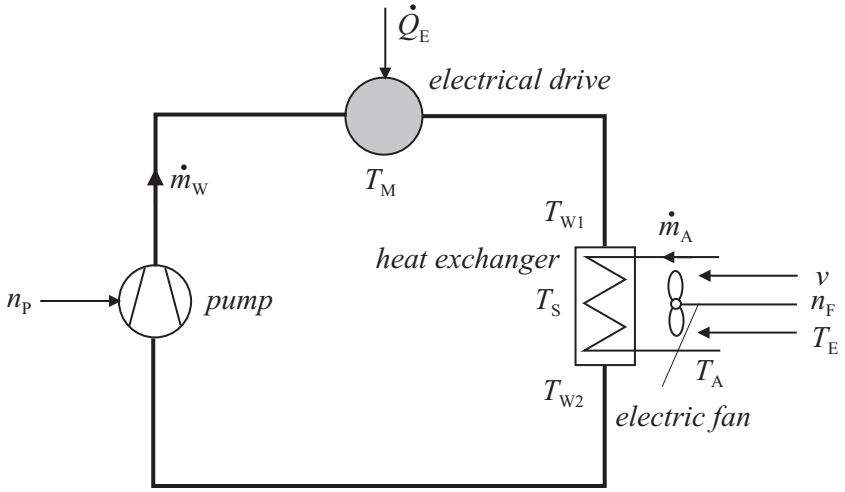

Figure 1: Cooling loop with two actuators

mathematical model can be derived:

$$\begin{aligned}
c_{p_M} M_M \frac{dT_M}{dt} &= -\alpha_{W1} A_{W1} (T_M - T_{W1}) + \dot{Q}_E \\
c_{p_W} M_{W1} \frac{dT_{W1}}{dt} &= \alpha_{W1} A_{W1} (T_M - T_{W1} - c_{p_W} (T_{W1} - T_{W2}) \dot{m}_W \\
c_{p_W} M_{W2} \frac{dT_{W2}}{dt} &= \alpha_{W2} A_{W2} (T_S - T_{W2} + c_{p_W} (T_{W1} - T_{W2}) \dot{m}_W \\
c_{p_S} M_S \frac{dT_S}{dt} &= -\alpha_{W2} A_{W2} (T_S - T_{W2} + \alpha_A A_A (T_A - T_S) \\
c_{p_A} M_A \frac{dT_A}{dt} &= -\alpha_A A_A (T_A - T_S) - c_{p_A} (T_A - T_E) \dot{m}_A
\end{aligned} \tag{1}$$

The parameters $c_{p_M}, c_{p_W}, c_{p_S}, c_{p_A}$ are the heat capacities of the masses and $\alpha_{W1}, \alpha_{W2}, \alpha_A$ denote heat transfer coefficients and A_{W1}, A_{W2}, A_A are the according contact areas. It is important that the heat transfer coefficients are depending on the mass flows which is taken into account in a simplified way by the following affine relations:

$$\alpha_{W1}(\dot{m}_W) = \alpha_{W1_0} + \alpha_{W1_1} \dot{m}_W \tag{2}$$

$$\alpha_{W2}(\dot{m}_W) = \alpha_{W2_0} + \alpha_{W2_1} \dot{m}_W \tag{3}$$

$$\alpha_A(\dot{m}_A) = \alpha_{A_0} + \alpha_{A_1} \dot{m}_A \tag{4}$$

Here $\alpha_{W1_0}, \alpha_{W1_1}, \alpha_{W2_0}, \alpha_{W2_1}, \alpha_{A_0}, \alpha_{A_1}$ are appropriately chosen constants. Furthermore it is assumed, that only $m+1$ distinct values can be selected for the rotational speed n_P of the pump. Therefore neglecting the dynamics of the pump the coolant mass flow $\dot{m}_W$ is considered to be a piecewise constant time function taking only $m+1$ distinct values a_i

$$\dot{m}_W(t) = \sum_{i=0}^{m} a_i d_i(t) \tag{5}$$

$$d_i(t) \in \{0,1\} \quad \sum_{i=0}^{m} d_i(t) = 1 \text{ for all } t. \tag{6}$$

Also the fan is assumed to operate at $n+1$ different stages only so that the air mass flow $\dot{m}_A$ can be represented as

$$\dot{m}_A(t) = \sum_{j=0}^{n} \left(c_{0j} + c_{1j} v(t)\right) e_j(t) \tag{7}$$

$$e_j(t) \in \{0,1\} \qquad \sum_{j=0}^{n} e_j(t) = 1 \text{ for all } t. \tag{8}$$

The constants a_i, c_{0j}, c_{1j} have to be determined from the pump and fan characteristics. Note that $\dot{m}_A$ also depends on the velocity v of the vehicle.

For the development and the realization of the control strategy a time discretization of the mathematical model is necessary. Since the thermal inertia of the air is much smaller than the thermal inertia of the other parts in the cooling system, i.e.

$$c_{PA} M_A \ll c_{PM} M_M, c_{PW} M_{W1}, c_{PW} M_{W2}, c_{PS} M_S,$$

model (1) is a *stiff* system of differential equations which would limit the time step size Δt drastically. Therefore the last differential equation in (1) is replaced by the algebraic equation

$$0 = -\alpha_A A_A (T_A - T_S) - c_{p_A} (T_A - T_E) \dot{m}_A. \tag{9}$$

With the definitions

$$\mathbf{x} := \begin{bmatrix} T_M & T_{W1} & T_{W2} & T_S \end{bmatrix}^T \quad \xi := \begin{bmatrix} \mathbf{x}^T & T_A \end{bmatrix}^T$$

the model can now be written as

$$\begin{aligned} \begin{bmatrix} \dot{\mathbf{x}} \\ 0 \end{bmatrix} &= \mathbf{A}_0 \xi + \mathbf{b}_0(t) + \sum_{i=1}^{m} \mathbf{A}_i \xi d_i \\ &\quad + \sum_{j=0}^{n} \left[\mathbf{b}_{1,j}(t) + \mathbf{B}_j(t) \xi\right] e_j \end{aligned} \tag{10}$$

with constant matrices $\mathbf{A}_0, \mathbf{A}_1, \ldots, \mathbf{A}_m$. The time dependent parameters $\mathbf{b}_0, \mathbf{b}_{1,0}, \ldots, \mathbf{b}_{1,n}, \mathbf{B}_0, \ldots, \mathbf{B}_n$ are determined by the external input functions $\dot{Q}_E(t), T_E(t), v(t)$. In *Kitanoski, F., and Hofer, A., 2010* a suitable procedure for the time discretization of (10) is presented leading to:

$$\begin{aligned} \begin{bmatrix} \mathbf{x}_{k+1} \\ 0 \end{bmatrix} &= \Phi \xi_k + \mathbf{h}_{0,k} + \sum_{i=1}^{m} \left(\mathbf{F}_i \xi_k + \mathbf{h}_{i,k}\right) d_{j,k} \\ &\quad + \sum_{j=0}^{n} \left(\mathbf{G}_{j,k} \xi_k + \mathbf{f}_{j,k}\right) e_{j,k} \end{aligned} \tag{11}$$

Here the notation $w_k := w(k\Delta t)$ for the value of a time function $w(t)$ at the time instant $k\Delta t$ is used. Additionally the power required to operate the pump at stage i is denoted p_i and the power used for the fan at stage j is q_j.

Based on this mathematical description the **energy optimal cooling problem** can be formulated:
Given the initial state $\mathbf{x}_0$ and the values of the external inputs $\dot{Q}_{E,k}, T_{E,k}, v_k$ for $0 \le k \le N$ (e.g. by measurements from a test cycle of N sampling periods), determine the binary valued variables

$d_{i,k}$ $i = 0,\ldots,m$ and $e_{j,k}$ $j = 0,\ldots,n$ for $0 \le k \le N-1$ such that the electrical energy used for the operation of the pump and the fan

$$E = \Delta t \sum_{k=0}^{N-1} \left(\sum_{i=1}^{m} p_i d_{i,k} + \sum_{j=1}^{n} q_j e_{j,k} \right) \tag{12}$$

is minimized subject to the constraints

$$T_{M,k} \le T_{\max} \quad \text{for } k = 1,\ldots,N \tag{13}$$

$$\left| T_{W1,k} - T_{W2,k} \right| \le \Delta T_{\max} \quad \text{for } k = 1,\ldots,N \tag{14}$$

where $T_{\max}$ and $\Delta T_{\max}$ denote some prescribed bounds.

Thus the temperature of the electrical drive must not exceed a given bound. The reason for the constraint (14) is mainly to avoid unrealistic solutions of the optimization problem. Note that in (12) the assumption $p_0 = q_0 = 0$ is posed, i.e. no power is required for stage 0 of the pump and the fan respectively.

3 Model predictive control strategy

In *Kitanoski, F., and Hofer, A., 2010a* it has been shown, how the energy optimal cooling problem can be converted to a mixed integer linear program (MILP) using some standard techniques from linear programming *Williams, H.P., 1999*. For this purpose global upper and lower bounds for the products $\mathbf{F}_i \xi_k$ and $\mathbf{G}_{j,k} \xi_k$ in (11) have to be determined. These bounds open the way to replace the bilinear terms in (11) equivalently by sets of linear inequalities. Based on the - of course - unrealistic assumption, that the external inputs $\dot{Q}_{E,k}, T_{E,k}, v_k$ for $0 \le k \le N$ are known in *advance,* it is possible to determine the global optimal solution. Although this approach cannot be used for a real application in a cooling management system immediately it provides valuable information to assess any cooling strategy from the energetic point of view.

In the sequel some results obtained for the cooling of the electrical drive in a parallel hybrid sport utility vehicle will be summarized. The external inputs for the example were taken from test bench measurements of a section of the New European Driving Cycle (NEDC). They are shown in Fig. 2.

Due to the implemented energy management system of the hybrid vehicle the electrical drive is mainly applied to boosting and energy recuperation. The following data were used for the pump and the fan

$$\begin{array}{lll} \text{pump:} & m = 2 & p_0 = 0,\ p_1 = 80,\ p_2 = 150 \quad [W] \\ \text{fan:} & n = 2 & q_0 = 0,\ q_1 = 250,\ q_2 = 550 \quad [W] \end{array}$$

and the constraints were chosen as

$$T_{\max} = 50\ [^\circ C] \qquad \Delta T_{\max} = 10\ [^\circ C]. \tag{15}$$

It is worth to note that starting from the initial condition

$$\mathbf{x}_0 = [\ 30 \quad 29.5 \quad 29 \quad 28.75\ ]^T \tag{16}$$

we get $\max T_{M,k} \approx 48.5\ [^\circ C]$ if the pump and the fan *always* operate at their *highest* levels. In this case the total amount of energy used for the cooling task within the period of 600 seconds

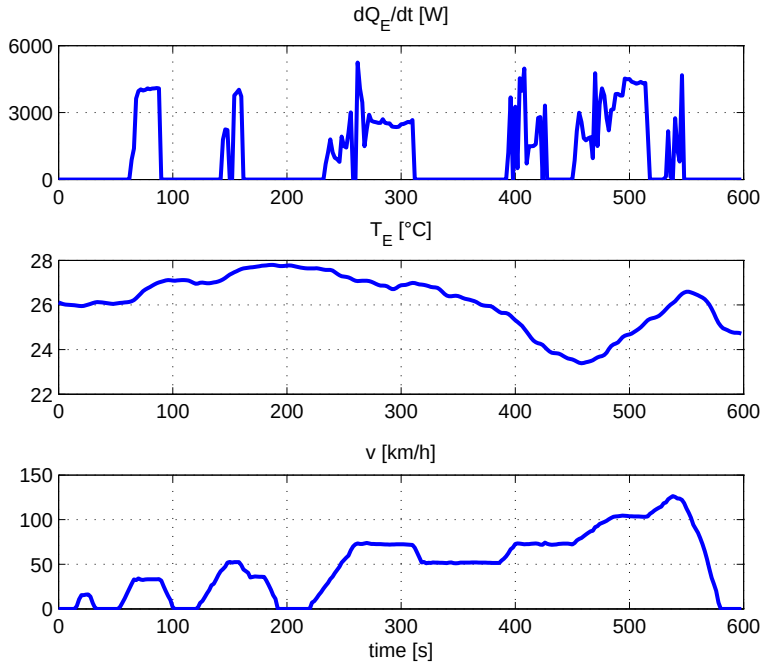

Figure 2: External inputs from a section of NEDC

is given by $E = 420\ [kJ]$. However the solution of the optimal cooling problem reveals that the required cooling can be accomplished with minimum energy

$$E^* = 148.8\ [kJ]. \tag{17}$$

It should be mentioned that the solution of this MILP problem with 900 integer variables and nearly 10000 continuous variables takes about 24 hours on a standard PC.

Now the development of a model predictive cooling control strategy is based on the following assumptions:

- At each sampling instant $k\Delta t$ the state $\mathbf{x}_k$ and the values of the external inputs $\dot{Q}_{E,k}, T_{E,k}, v_k$ are known from measurements.
- Although there are many contributions dealing with the benefits of prediction in model predictive control concepts for automotive applications (see e.g. *Katsargyri, G.E. et al., 2009* or *Van Keulen, T., et al., 2010*) no such techniques should be incorporated in the present case in order to keep the cooling strategy as simple as possible.

As a first step for the development of a control scheme an analysis of the steady state behavior of the continuous time model (1)-(8) for constant external inputs

$$\dot{Q}_E = 2500\ [W] \text{ for all } t \geq 0$$
$$T_E = 20\ [^\circ C] \text{ for all } t \geq 0$$

and constant pump and fan stage selections is performed. The chosen value of $\dot{Q}_E$ approximately corresponds to the mean value of $\dot{Q}_E$ from the NEDC example if only values different

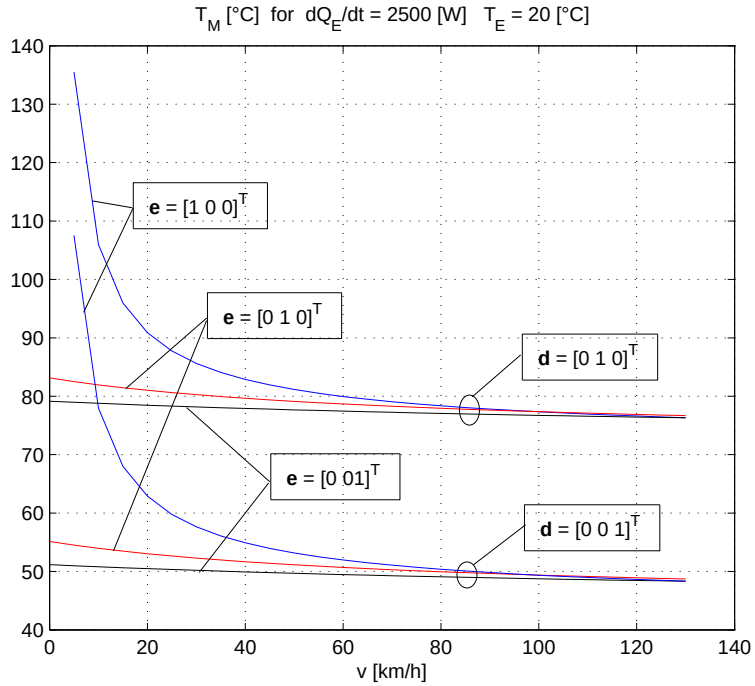

Figure 3: Steady state values of T_M

from zero are taken into account. If all external inputs and the control inputs are constant the equations (1)-(8) describe an asymptotically stable linear time-invariant system. Setting all time derivatives in (1) to zero we can solve the resulting algebraic equations for the steady state values of $T_M, T_{W1}, T_{W2}, T_S, T_A$. Since the cooling effect of the air mass flow $\dot{m}_A$ also depends on the velocity v this procedure has been carried out for different values of v within the range $0 \leq v \leq 130\ [km/h]$. The results for the temperature T_M are shown in Fig. 3.

Here for convenience the following notation for the control inputs

$$\mathbf{d} := \begin{bmatrix} d_1 \\ d_2 \\ d_3 \end{bmatrix} \quad \mathbf{e} := \begin{bmatrix} e_1 \\ e_2 \\ e_3 \end{bmatrix}$$

is used. Now it becomes obvious that the fan should be activated only at low speed of the vehicle. Fig. 3 also reveals that the prescribed bound (15) for T_M will cause severe problems for the control strategy. Due to economical reasons the cooling system for the electrical drive has been deliberately small sized in the present case.

Now based on the results shown in Fig. 3 it is reasonable to introduce a velocity dependent term *maximum cooling* which is defined as:

$$\begin{aligned} &\textit{maximum cooling:} \\ &\mathbf{d} = [\ 0 \quad 0 \quad 1\ ]^T \text{ and} \\ &\begin{cases} \mathbf{e} = [\ 0 \quad 0 \quad 1\ ]^T & \text{if} \quad v \leq 20 \\ \mathbf{e} = [\ 0 \quad 1 \quad 0\ ]^T & \text{if} \quad 20 < v < 80 \\ \mathbf{e} = [\ 1 \quad 0 \quad 0\ ]^T & \text{if} \quad v \geq 80 \end{cases} \end{aligned} \tag{18}$$

On the other hand the term *no active cooling* is obviously given by

$$\begin{array}{l} \textit{no active cooling:} \\ \mathbf{d} = \left[\begin{array}{ccc} 1 & 0 & 0 \end{array}\right]^T \text{ and } \mathbf{e} = \left[\begin{array}{ccc} 1 & 0 & 0 \end{array}\right]^T \end{array} \tag{19}$$

If we remember the results from the classical fuel optimal control problem *Athans, M., and Falb, P.L., 1966* where the optimal control is determined via the so-called dead zone function (i.e. the optimal control is either zero or takes its maximum/minimum value) the significance of *maximum cooling* and *no active cooling* for the cooling strategy to be determined becomes evident.

The next investigation deals with the dynamic behavior of the temperature T_M. It should be figured out what is the increase of T_M in the worst case. For this purpose a pulse for the external thermal load determined as $\dot{Q}_E = 4000\ [W]$ for $0 \leq t \leq 40$ is considered which approximately corresponds to the maximum load during the NEDC (see Fig. 2). The environmental temperature is kept constant at $T_E = 20\ [^\circ C]$. Both the pump and the fan permanently operate at the highest level, which has the consequence that the velocity v has only a minor impact on the temperatures. Starting from different initial conditions the simulation of the cooling system reveals that T_M increases about 15 $[^\circ C]$ in the worst case. This observation gives the advice to augment the cooling strategy in the following way: Choose a *safety gap*

$$s \approx 15\ [^\circ C]$$

and try to keep the temperature T_M below $T_{\max} - s$ during periods in which no or only minor cooling is required. In doing so the cooling system can cope with the hard bound $T_M \leq T_{\max}$ during worst case thermal loads.

Now we are ready to formulate the proposed model predictive cooling strategy based on an appropriately chosen receding horizon of P sampling instants. The concept contains two major mathematical modules, which are carried out starting from the available information about the actual state $\mathbf{x}_k$ and the actual values of the external inputs $\dot{Q}_{E,k}, T_{E,k}, v_k$:

- simulation of the discrete time model (11) with fixed control inputs *maximum cooling* or *no active cooling* for the receding horizon P
- solution of the (small size) mixed integer linear programming problem for energy optimal cooling during the receding horizon P

It is a common feature of both modules that the external inputs $\dot{Q}_{E,k}, T_{E,k}, v_k$ are considered to be *constant* during the receding horizon. As it has been already mentioned above it might be possible to improve the control scheme applying some method to forecast the external inputs. The results produced by the simulation module are checked for the prescribed constraints (13,14) and the quantities

$$\Delta T_{M,i} = T_{M,i} - T_{\max} \quad \text{for } i = 1, \ldots, P$$

are determined. The solution is termed "OK" if the conditions

$$\begin{array}{c} \max\limits_i \Delta T_{M,i} \leq 0 \\ \left| T_{W1,i} - T_{W2,i} \right| \leq \Delta T_{\max} \quad \text{for } i = 1, \ldots, P \end{array}$$

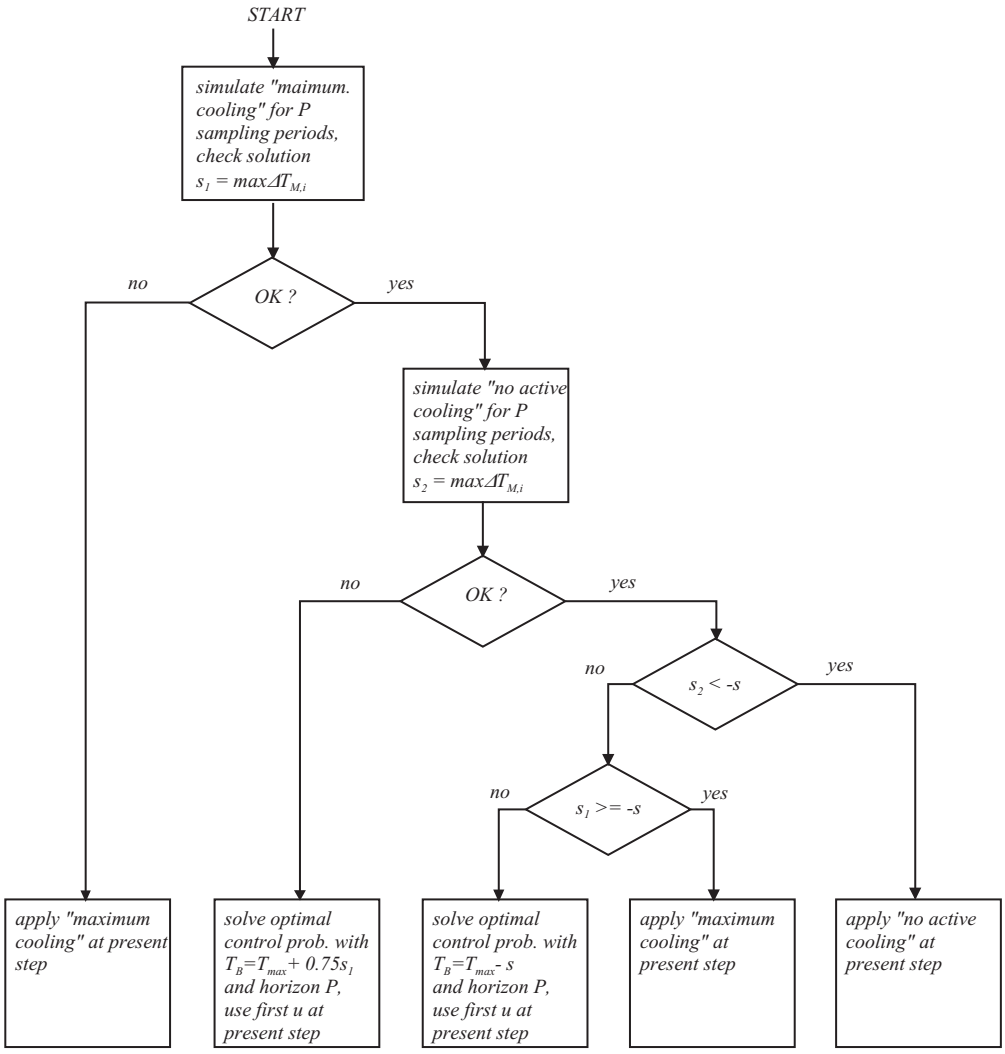

Figure 4: Model predictive control strategy

are satisfied. The optimization module uses a dynamically adapted bound T_B instead of $T_{\max}$ to limit the temperature T_M. This feature has proven to be useful in order to maintain the safety gap and to guarantee feasible solutions of the optimization problem in any case. The result of the optimization module is given by an optimal sequence for the control inputs which are collected in a vector for notational convenience

$$\mathbf{u}_i := \begin{bmatrix} \mathbf{d}_i \\ \mathbf{e}_i \end{bmatrix} \quad \text{for } i = 0, \ldots, P-1.$$

Only the first element $\mathbf{u}_0$ of this sequence is applied as control input to the plant at the current sampling instant.

Now the model predictive cooling control concept can be summarized as follows:
Given the state $\mathbf{x}_k$ and the values of the external inputs $\dot{Q}_{E,k}, T_{E,k}, v_k$ at the actual time instant $t = k\Delta t$ perform the computations depicted in the flow chart shown in Fig. 4. Apply the determined control input to the plant until the next sampling instant.

Remarks:
The proposed strategy differs significantly from conventional model predictive control schemes where a certain optimization problem is solved at *each* sampling instant. In these cases stability of the closed loop system can be enforced by an appropriate choice of the objective functional or by suitable terminal constraints (see e.g. *Maciejowski, J.M.,2002*, *Mayne, D.Q., et al., 2000*). In the present case the main demand is to keep the temperature T_M below a prescribed bound with a minimum amount of energy. The proposed concept is build up by a mixture of simulation and optimization steps and the objective used in the optimization is only determined by the control input. No state information is included and also terminal constraints are not applicable. As a consequence a rigorous proof of stability cannot be provided. Of course this is a severe shortcoming from the theoretical point of view but keeping in mind the practical aspects one can get over this drawback especially if the slow dynamics of the plant is considered.

4 Numerical Results

In order to demonstrate the performance of the proposed model predictive cooling strategy a simulation of the closed loop cooling system with the external inputs shown in Fig. 2 is performed. The sampling period Δt for the controller and the horizon P are chosen as

$$\Delta t = 4\ [s] \tag{20}$$

$$P = 5 \tag{21}$$

This choice for the MPC horizon is motivated by the dynamic properties of the plant and the fact that no prediction method for the external inputs is included in the control concept. Furthermore the size of the resulting optimization problem should be small in order to keep the required CPU time modest. With the initial conditions (16) the behavior of the closed loop control system is shown in Fig. 5.

A minor violation of the constraint posed on T_M can be detected in Fig. 5 but considering the uncertainty of the model this fact has no real impact from the practical point of view. The second diagram in Fig. 5 confirms that the constraint (14) is also met by the solution. Remember that this constraint was primarily introduced to obtain reasonable solutions of the energy optimal feed forward control problem. Obviously it has less importance for the model predictive control. The pump and fan stage selection resulting from the model predictive control scheme is presented in figure 6.

The energy consumption of the model predictive control in this scenario is

$$E = 185.12\ [kJ]$$

which is quite satisfactory compared to the optimum value $E^* = 148.8\ [kJ]$. Once again it must be emphasized that the optimum value is obtained using the knowledge of the external inputs over the total time interval of interest in advance.

Finally some remarks about the implementation of the proposed MPC scheme are appropriate. The sampling period (20) is large enough such that standard ECU hardware used in automotive applications seems to be adequate. This is definitely true for the simulation module of the control strategy. However the optimization module requires the solution of a mixed integer linear program. The number of integer variables which is crucial for the required CPU time is 30 for the chosen optimization horizon. In the actual optimization problem the integer

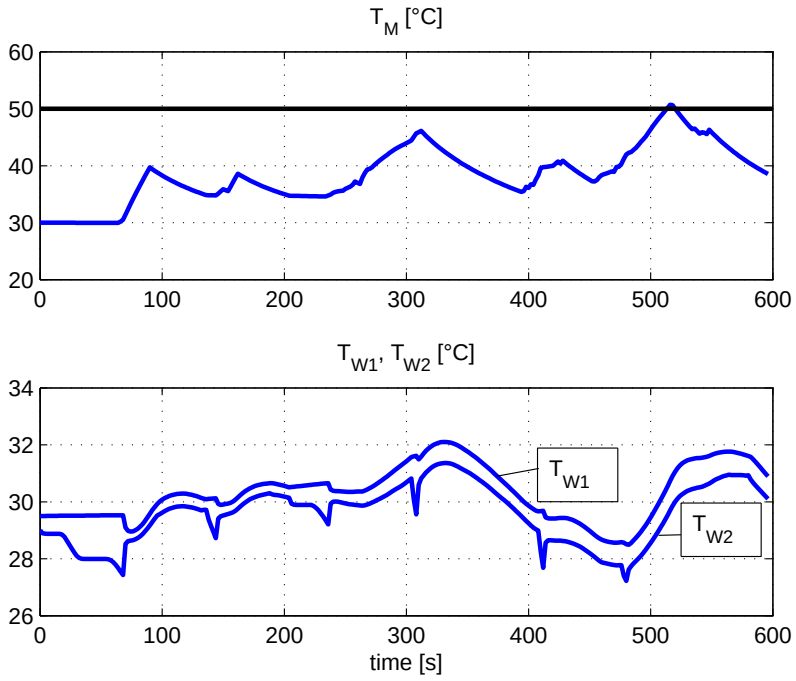

Figure 5: Results of model predictive control

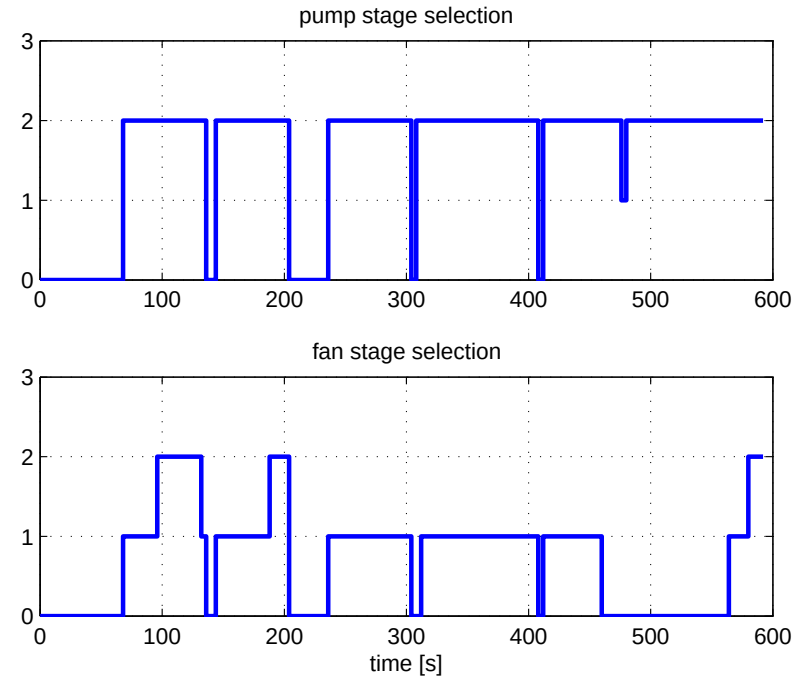

Figure 6: Pump and fan stage selection of model predictive control

variables are the components of $\mathbf{d}_i$ and $\mathbf{e}_i$ and the equations (6), (8) imply that at each sampling instant exactly one component has to take the value 1. Therefore these vectors can be treated as so-called special ordered sets of type 1 (see e.g.*Beale, M.L., Forrest, J.J.H, 1971*. Standard solvers for mixed integer linear programs, for example CPLEX *IBM Corp., 2009* can exploit special ordered sets to accelerate the solution process. Furthermore it is also important that this mixed integer linear program always has a *known* feasible solution. Experiments with a standard PC hardware and the solver CPLEX have shown that the optimization module typically requires CPU times of about 0.5 to 1 seconds. This might seem unduly long but the CPU time can be further reduced essentially if the solver is not forced to determine the optimal solution and instead suboptimal solutions (with a prescribed suboptimality level) are accepted. Of course a reduction of the horizon will lead to a smaller optimization problem and consequently to shorter CPU times as well.

5 Conclusion

A model predictive control strategy for the cooling of an electrical drive in a hybrid electrical vehicle has been presented. It can be regarded as a first step towards an energy efficient cooling on demand concept. Since in some situations the controller requires the solution of a mixed integer linear program a powerful hardware and a state of the art solver software are indispensable prerequisites for the implementation. Typically the MILP has to be solved at about 20 percent of all sampling instants. Therefore future investigations will aim at the question how to eliminate the optimization module from the concept at all.

Acknowledgement
This work was partly supported by the "COMET K2 Forschungsförderungs - Programm" of the Austrian Federal Ministry for Transport, Innovation and Technology (BMVIT), the Austrian Federal Ministry of Economics and Labour (BMWA), Österreichische Forschungsförderungsgesellschaft mbH (FFG), Das Land Steiermark, and Steirische Wirtschaftsförderung.

References

[1] ATHANS M., FALB P.L.: Optimal Control: An Introduction to the Theory and Its Applications, McGraw-Hill Book Company, New York, 1966.

[2] BEALE E.M.L., FORREST J.J.H.: Global Optimization Using Special Ordered Sets, Mathematical Programming, Vol. 10, 1971, pp. 52 - 69.

[3] CAMACHO E.F., BORDONS C.: Model Predictive Control, Springer, New York, 1999.

[4] IBM CORP.: Users's Manual for CPLEX, 2009.

[5] KATSARGYRI G.E., KOLMANOVSKY I.V., MICHELINI J., KUANG M.L., PHILIPS A.M., RINEHARD M., DAHLEH M.A.: Optimally Controlling Hybrid Electric Vehicles Using Path Forecasting, Proc. of American Control Conference, 2009, pp. 4613 - 4617.

[6] KITANOSKI F., HOFER A.: Energy Optimal Control of a Cooling System - Limits of Performance, Proceedings of the Int. Conf. Modelling, Identification and Control (MIC 2010), Innsbruck, Austria, 2010, pp.116 - 121.

[7] KITANOSKI F., HOFER A.: A Contribution to Energy Optimal Thermal Management for Vehicles, IFAC Symposium Advances in Automotive Control (AAC 2010), Munich, Germany, 2010.

[8] MACIEJOWSKI J.M.: Predictive Control with Constraints, Pearson Education Limited, Harlow, 2002.

[9] MATTINGLEY J., WANG Y., BOYD S.: Code Generation for Receding Horizon Control, Proc. of 2010 IEEE Int. Symposium on Computer-Aided Control System Design, Yokohama, Japan, 2010, pp. 985 - 992.

[10] MAYNE D.Q., RAWLINGS J.B., RAO C.V., SCOKAERT P.O.M.: Constraint Model Predicive Control: Stability and Optimality, Automatica, Vol.36, 2000, pp.789 - 814.

[11] VAN KEULEN T., DE JAGER B., KESSELS J., STEINBUCH M.: Energy Management in Hybrid Electric Vehicles: Benefit of Prediction, IFAC Symposium Advances in Automotive Control (AAC 2010), Munich, Germany, 2010.

[12] WILLIAMS H.P.: Model Building in Mathematical Programming, John Wiley & Sons, New York, 1999.

Cost Oriented Humanoid Robot Archie

Siavash Dezfouli [1], Peter Kopacek [1], Mohsen M. Daniali [1]

[1] Intelligent Handing and Robotics (IHRT), Vienna University of Technology

siavash.dezfouli@gmail.com, kopacek@ihrt.tuwien.ac.at

Abstract-*Robotics can be regarded as a typical and representative part of Mechatronic, as a cutting edge technology in this rapidly expanding research field. Hence on the tree of robotic life, humanlike robots play a particularly valuable role.*
This Paper deals with design of cost oriented teen sized humanoid robot Archie. It describes the mechanical and electrical components and how action commands are transmitted from PC to motion controller which controls each motor in joint via universal serial bus (USB) to Control Area Network (CAN) bus converter. The mechanical structure has the following features: teen sized, light weight, low power consumption, low cost.
The teen sized humanoid robot Archie is in development as a collaboration of Vienna University of Technology, University of Manitoba in Canada and National Kaoshiung First University for Science and Technology in Taiwan. Main goal is to develop a cost oriented autonomous humanoid robot to assist human in daily life tasks.

1 Introduction

Humanoid robots have been attracting great attention among robotic scientists since 1973 when the first full-scale anthropomorphic robot was built (www.inlportal.inl.gov, 2011). From the early simple design, humanoid robots have improved rapidly to imitate the human behavior due to progress in material sciences, electric motors, sensors and computer science. These improvements have led to design more autonomous anthropomorphic robots. In addition to walking, these humanoid robots can exhibit emotion, forge relationships, make decisions, and develop as they learn through interaction with the environment. In fact the final goal of these projects is to build the human-like robot to interact with people.
However, many humanoid robots was designed and constructed in well-founded companies and research labs due to the requirement of complicated and expensive devices. In order to build a cost-oriented humanoid robot, many researchers have been done in these years. These new generation of humanoid robots have been used in different international competition in all over the world. These competitions cause a great progress in this field because they provide good conditions to compare the robots in real-world environment. This progress help researchers to design more adaptive and flexible humanoid robot in different situation to reach final goal that would be the interaction with human.
Furthermore, humanoid robot is a complex system that combine diversified disciplinary such as mechanics, electronics, control, computer programming, artificial intelligence, etc. first of all the mechanical design of robot should be designed such that the robot would be robust enough to perform different tasks. After that the electric actuator is designed and installed in each joints to produce enough force to move different links of robot. Finally the important part is to design a

high level control system to send commands through connections for electric devices to activate them. The final part of the robot has the most sophisticated design among other sections that plays role of brain in robot.
This paper introduces the design of cost oriented teen sized humanoid robot Archie. It describes the mechanical and electrical components and how action commands are transmitted from PC to motion controller which controls each motor in joint via universal serial bus (USB) to Control Area Network (CAN) bus converter. The control system used in Archie is based on distributed star bus architecture. In this composition, each single joint is controlled separately by a motion controller which receives low level movement and status commands from a PC (Dezfouli, 2011).

2 Mechanical design

In order to design a mechanical system for a humanoid robot, a complex and careful compromise between different factors such as form, function, weight, cost and manufacturability is required. The mechanical structure of Archie is designed and built with aluminum material such that in addition to rigidity, its weight remains less than 30 Kg. Based on this design the height of robot is about 1.2m. The mechanical structure is considered to be fundamentally comprises of human size, low weight, low power consumption, low cost and uniquely mimic to a human physical body as illustrated in Fig. 1.

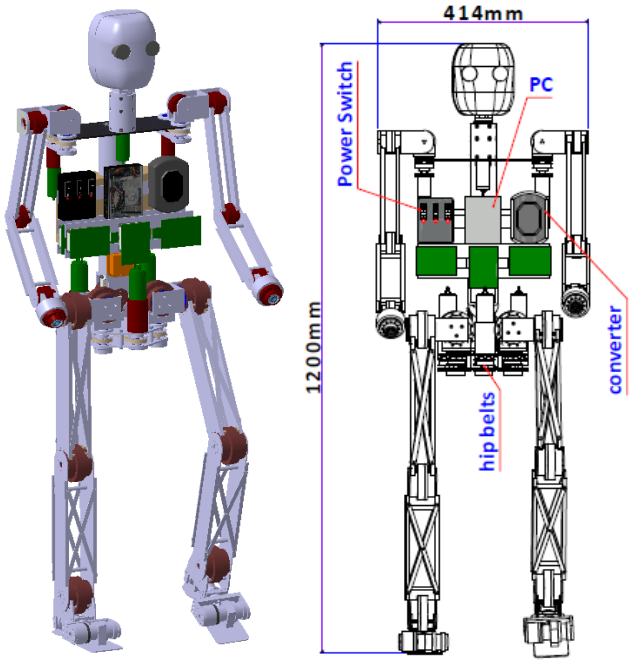

Figure 1: Archie mechanical design and structure

Furthermore, we choose gears and harmonic drives within design parameter such as space, shape, permissible power, weight and etc. For actuator a combination of brushless and servo DC

motor is used based on the joint circumstances. For communication, CAN bus network is selected and implemented in Archie to send the commands quickly from motion controller to joints. A high level motion controller that runs in a laptop is designed to create appropriate desired command for each joint to guarantee the stability of dynamic walking. Each joint has additionally its own control system that includes a PID controller and encoder. Finally two 14.4 volts batteries generate the required energy for electric motors.

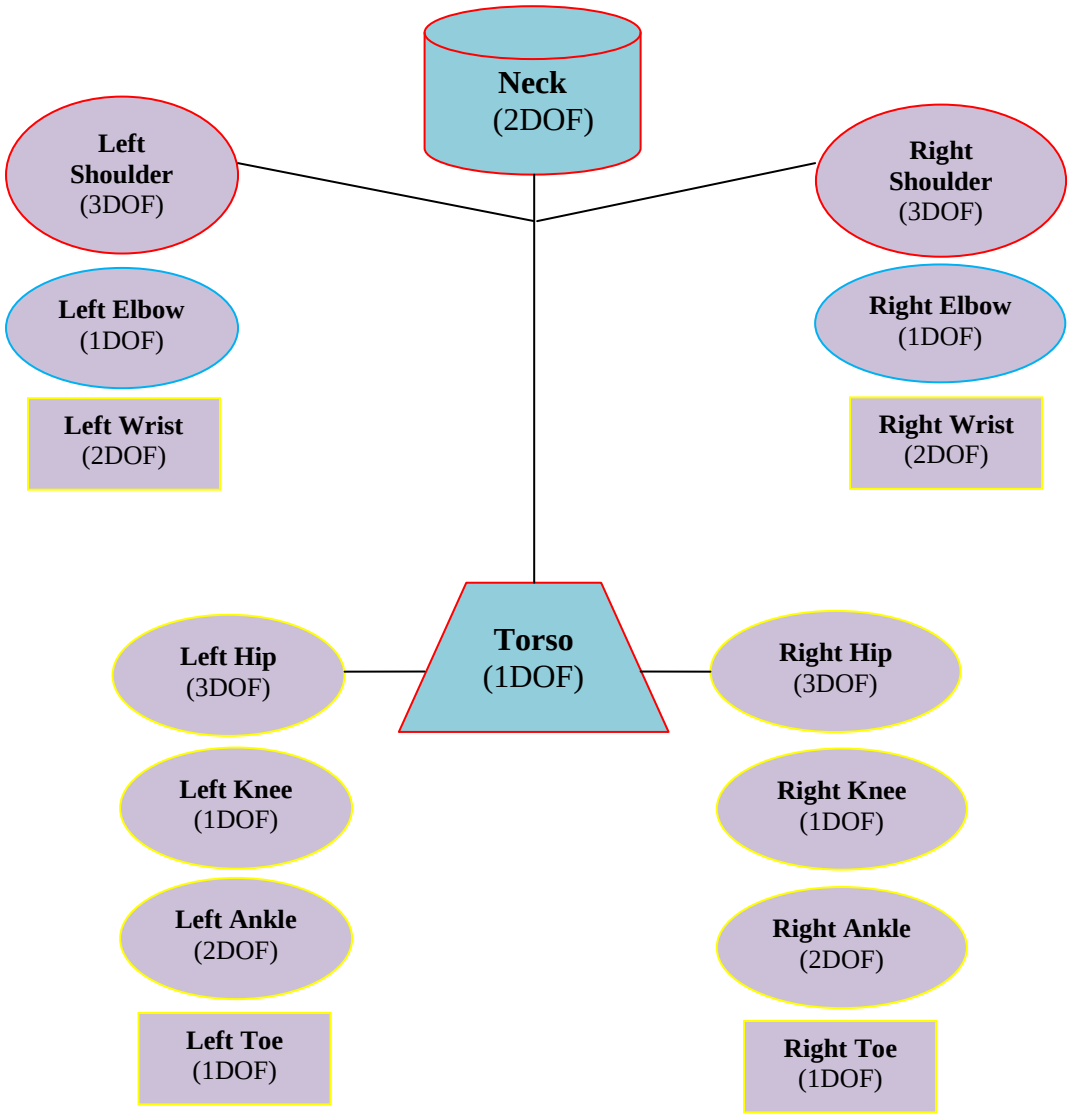

Figure 2: Schematic kinematic design of Archie

As depicted in Fig.2, Archie has totally 29 degree of freedom (DOF). These are 7 DOF in each leg. The torso also has two DOF to make it able to rotate the upper body. The other 13 DOF is related to upper body; six DOF for each hand and two DOF for the neck. The 3 DOF joint -i.e. spherical joint- in shoulder give enough capability to hand to move in space in each desired position. The aforementioned kinematics make the Archie capable to perform dynamic walking smoothly while do other tasks with upper body. One of the most outstanding characteristic of Archie is that it has ability to actuate its toes, which allow it to roll over the foot during walking.

3 Electrical design

As it is mentioned before, there are two different motors that are used in Archie to actuate the joints; brushless motor and DC servo motor. The brushless motor has some advantages such as high efficiency and less noise that make it clearly as an unavoidable choice for humanoid robot. Although the control scheme of brushless motor is a bit complex, it allows to fine control of joint. This factor is essential especially for those joints of robot that play role for walking.

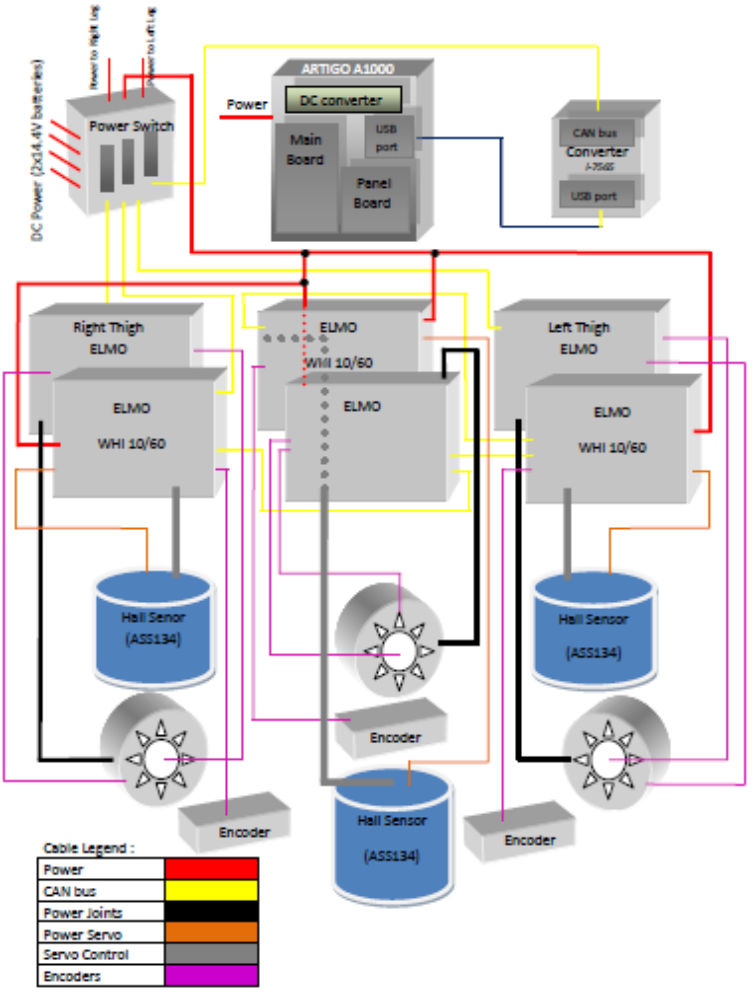

Figure 3: Upper body cable map connection

On the other hand, the brushless motors are more expensive especially for those that create great torque. Therefore we used DC servo motor for some joints that need more torque such as in torso.

Figure 3 and 4 illustrate the connection and performance of implemented distributed controller of Archie for upper and lower body, respectively. Upper body of Archie is included motion controller to control motor drives in hip and torso, data converter, power switch, and encoders. These components are connected via specific cables due to their task. Each motor is connected by encoder, power and communication cables to motion controller. In order to control of a humanoid robot that has a complex and coupled kinematics and dynamics, a complicated control scheme is needed. The proposed controller for Archie is based on the distributed control strategy. In this method, every joint has its own control that controls the position and velocity of it. In order to achieve this goal, the digital servo motor drive so called Whistle is used.

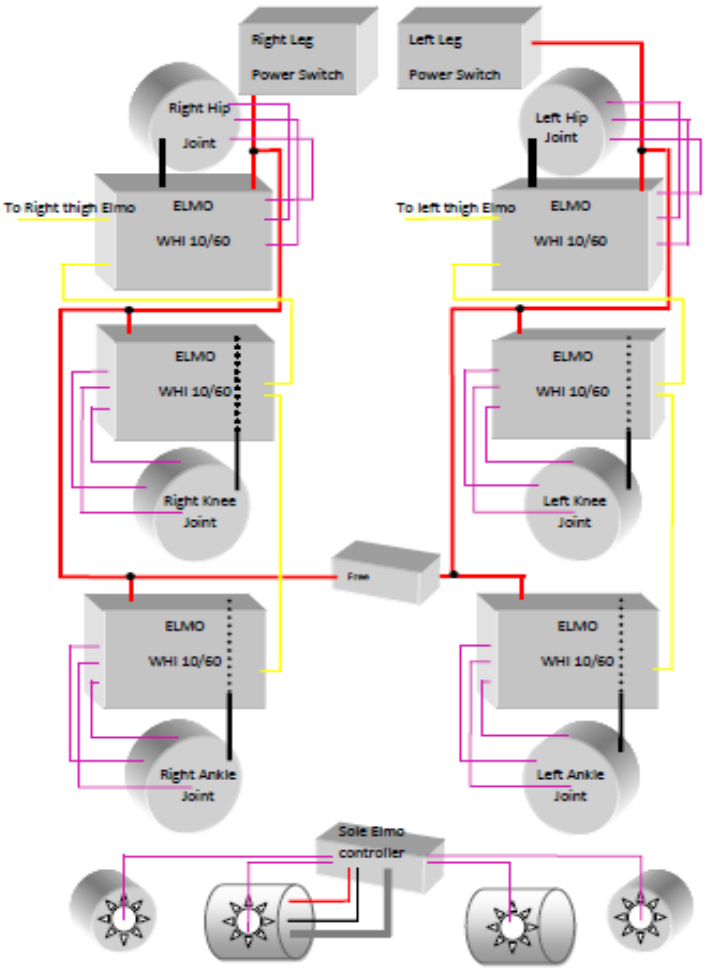

Figure 4: Lower body cable map connection

Cable connections between electrical components are similar to upper body, in this connection each single motor is connected to its own motor drive and PCB (Printed Circuit Board). The Whistle is a series of intelligent miniature digital servo drives for DC brush and brushless motors, linear motors and voice coils. Otherwise, another high level control that implemented by laptop send the desired command to each joint controller to confirm stability of robot in walking.

4 Communication design

For the communication in our robot action commands are sent from PC to USB-CAN converter. The aim of using such a communicator in our robot is that it provides the error process mechanisms and message priority concepts. On the other hand it can transmit messages in real-time; meaning that the message with the highest priority will be delivered within a guaranteed latency time.

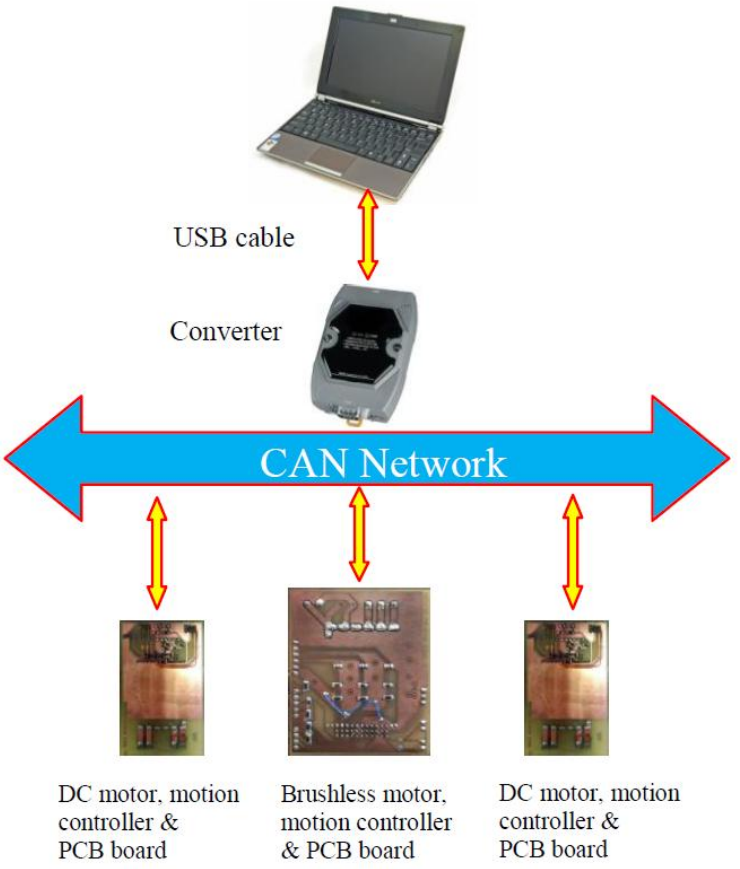

Figure 5: Communication architecture

The Controller Area Network is a serial bus communication protocol, which efficiently supports distributed real-time control with a very high level of security. CAN communicator which is

used in Archie is ideally suited in applications requiring a large number of short messages with high reliability in rugged operating environments.
Because CAN is message based and not address based, it is especially well suited when data is needed by more than one location and system-wide data consistency is mandatory. The CAN system we implemented uses two wires in its cable, one for a dominant state and one for a recessive state. These messages transmitted to motion controller by CAN cables to set up and control the joints and activate the motor drivers for robot motion (see Fig. 5).

5 Motor Drivers

Motion controller is a world leader in the development and manufacture of advanced technology in motion control that includes ultra-compact, high power density digital servo drives and innovative network motion controllers.
Motion controller servo drives combine high power density, intelligent functionality and space-friendly design. The drives integrate motion controllers advanced, which enables superior control performance, offers advanced programming capabilities and supports standard communication protocols. All the drives in the series include a fully digital motion controller that features current, velocity and position loops and a wide range of commutation types and position feedbacks.

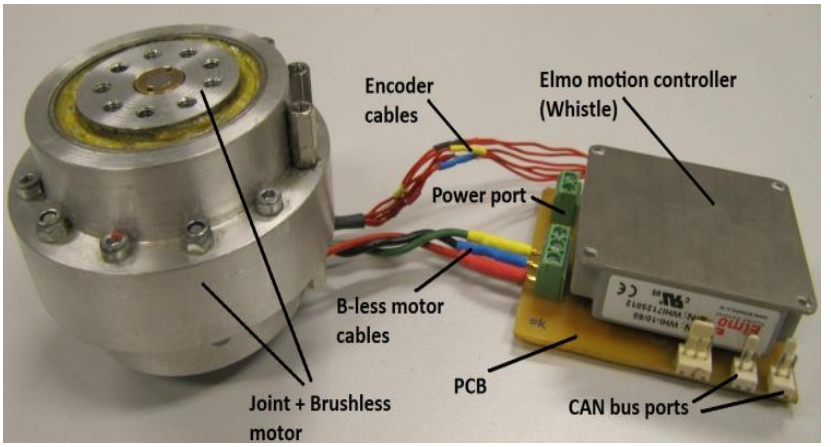

Figure 6: Motion controller mounted on a PCB and connected to brushless motor inside the joint

The type of motion controller we used is a series of intelligent miniature digital servo drives for the current DC and brushless motors of Archie. The matchbox-sized servo drive weighs only 1.8 oz (50 g) and supports up to 20 amps continuous current. Its high density allows the drive to deliver a peak of 3200 W of power and 1600 W of continuous power (www.elmomc.com/products/elmo-digital-servo-drives-ExtrIQ). The motion controller is a PCB (printed circuit boards) mounted device (see Fig. 6) that enables efficient and cost saving implementation.

One of the latest improvements in motor drives for teen sized humanoid robot is new designed PCB for brushless motors (see Fig. 7). In this design, connection of cables and encoder are improved in a way that it needs less space and much easier soldering.

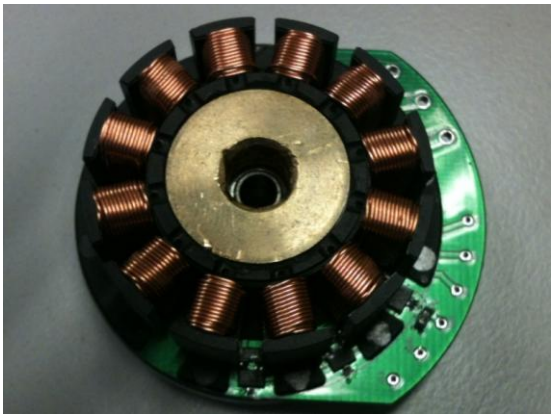

Figure 7: New design for brushless motor board

6 Simulation and interface design

In order to control the robot some parameter should be selected before real performance. These parameter are included information such as type of communication, baud rate, kinematic (i.e. hip height, amplitude, sway range, joints length and width dimensions,...), walking steps parameters, and finally angle values modification for testing and implementing of each joints for movement.

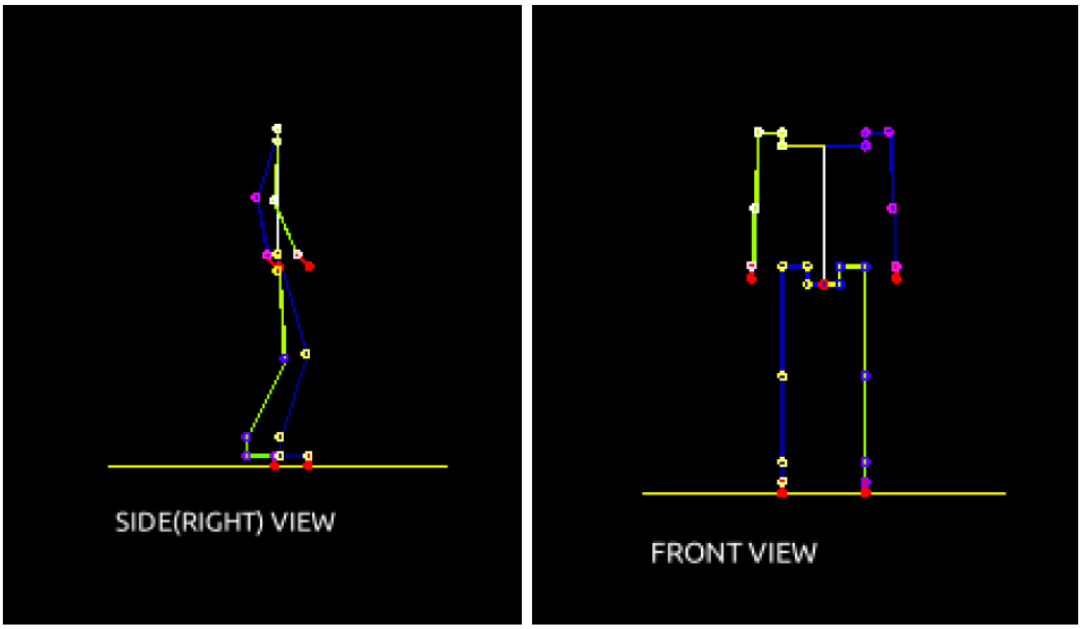

Figure 8: Walking simulation in side and frontal view

Our motion controller program is designed based on locomotion of Archie in forward, backward, leftward and right ward walking. It is also included important parameters that should be tuned according to hardware and design of robot to control the locomotion.
Since each joint is basically connected to motion controller program via the proposed communication interface for an individual motion, the interface should provide appropriate setting ability for position and velocity profile of each joint in Archie to manage the proper movement. Besides the kinematic/dynamic information in motion controller program of Archie there are graphs and motion simulator for designing a model of an actual and physical behavior of robot, to execute the movement commands, and test and analyze the execution output.
These simulations let you play robot in a virtual world and provide you a better vision that can avoid injuries and damages and necessary or unnecessary changes in design of the robot as demonstrated in Fig. 8.

Conclusion and future works

The main goal is to develop a cost oriented autonomous humanoid robot to assist human in daily life tasks. We have presented our mechanical design, communication interface and motion controller program respect to the humanoid robot Archie which moves like a human. We chose the CAN bus because of the robustness compared with Recommended Standard (RS) 232 that we used already. Furthermore, the CAN bus provides hardware support for priority based messaging and filtering of messages.
Finally it should be mentioned that Archie motion control program is under the test and development.

References:

Dezfouli,S., Kopacek,P. (2011). “Mechatronic Design of Humanoid Robot Archie”- 20th International Workshop on Robotics in Brno-Czech Republic. Oct.2011.

Elmo motion controller (Whistle), July 2010, www.elmomc.com.

Idaho National laboratory, 2011. Humanoid Robotics. Webpage, (www.inlportal.inl.gov) Last visited on November 2011.

Positive Realness and Positive Definiteness: Gradients and Robustness

Alexander Weinmann, OVE, Senior Member IEEE
Vienna University of Technology, Institute of Automation and Control
Gusshausstrasse 27-29/376, A-1040 Vienna / Austria
Phone: +43 1 58801 37611, Fax: +43 1 58801 37699
email: weinmann@acin.tuwien.ac.at

Manuscript received May 18, 2011

Abstract

Positive realness is extended for application-oriented purposes in this article. With the help of symbolic computation, the positive realness conditions are automatically generated. The regions of positive realness are investigated in the parameter plane. In the presence of parameter uncertainties, the realness conditions are studied in order to develop robust algorithms. An extension of positive realness is set up where positive realness is aimed at in a predetermined lowpass frequency region. Furthermore, gradients are presented to approach positive realness conditions for applications with arbitrary data, which can be determined in parts.

Eventually, positive definiteness of a matrix is obtained by using gradients with respect to an auxiliary matrix which influences especially the worst subdeterminant of the matrix. This method is used in the field of Lyapunov stability and hyperstability.

Several examples are presented for the illustration from a engineering point of view.

Keywords: Permitted regions for positive realness, symbolic deconvolution, lowpass positive realness, conditions for negative imaginary functions, hyperstability requirements

1 Introduction

Positive realness has become an interesting field of research in the last decades. Especially the correspondence with passive networks has been a challenge. There is a huge quantity of references dealing this matter (e.g., *Adamy, J., 2009; Ljung, L., 1977; Lozano-Leal, R., and Joshi, S.M., 1990; Marquez, H.J., and Damaren, C.J., 1996* and several cited at the end of the References).

In the following sections, the general matrix $\mathbf{A}$ is a replacement of an open-loop or closed-loop system $(\mathbf{A} + \mathbf{BK})$ under discussion, where some changes in the parameters (mostly of the controller part $\mathbf{K}$) are possible and intended in order to satisfy positive real requirements.

A lot of important results is now reviewed for introductory purpose (*Föllinger, O., 1993; Petersen, I.R., and Lanzon, A., 2010*).

The scalar complex transfer function $G(s)$ is (strictly) positive real if in the open right half-plane

$$\Re e\ G(s)\Big|_{\Re e\ s>0} > 0\ . \tag{1}$$

The following properties are recalled: This is satisfied if $G(s)$ is stable. Poles at the imaginary axis must be simple and characterized by positive residues. If there is no pole at the origin, positive realness is also given for $\Re e\ G(j\omega)\Big|_{\omega\geq 0} \geq 0$. Zeros in the right half-plane are not permitted. The difference of the degrees of the numerator and denominator polynomial of $G(s)$ is 0 or 1. Positive real functions occur as the inverse complex admittance in an electrical network with only passive elements. In addition, $G(s)$ is *strictly* positive real if no zero or pole at the imaginary axis exists.

A matrix $\mathbf{G}(s)$ is positive real if for an arbitrary complex vector $\mathbf{z} \neq \mathbf{0}$

$$\Re e\ [\mathbf{z}^H \mathbf{G}(s)\mathbf{z}]\Big|_{\Re e\ s>0} > 0\ , \quad \mathbf{z}^H \equiv (\mathbf{z}^*)^T\ . \tag{2}$$

There are the following correspondences: The matrix $\mathbf{G}(s)$ is positive real if the corresponding Hermite part $\mathbf{G}_H(s) \stackrel{\triangle}{=} 0.5[\mathbf{G}(s) + \mathbf{G}^*(s)]$ is positive real. $\mathbf{G}_H(j\omega)$ must be Hermite and positive definite for $\omega \geq 0$. The elements of $\mathbf{G}(s)$ must satisfy the conditions for positive real scalar transfer functions. Based on the conditions of square functions in $\mathbf{z}$, the property positive real corresponds to the property of positive definiteness of the Hermite part $\mathbf{G}_H(s)$, i.e., all the northwest subdeterminants are positive. Positive definite is given for > 0, positive semi-definte for ≥ 0. A Hermite matrix is positive definite (semi-definite) if all the eigenvalues are > 0 (≥ 0). Moreover, all the main diagonal elements must be positive.

Remind the conditions for hyperstability: The LTI system $\mathbf{G}(s)$, see Eq.(64), is hyperstable (asymptotically hyperstable) if the Popow integral equation

$$\int_0^t \mathbf{u}(\tau)^T \mathbf{y}(\tau)^T d\tau < \varepsilon_0^2, \quad t \geq 0 \tag{3}$$

is satisfied for positive and constant ε_0 and if $\mathbf{G}(s)$ is positive real (strictly positive real).

Considering positive realness, one has to keep in mind that positive realness might be accompanied by some problems in industrial applications, even in simple ones. To guarantee positive realness the difference of the numerator and denominator degree must not exceed one. From purely mathematical viewpoint this is easy. In applications, this is achieved (1) by introducing elements with differentiation property or (2) by switching proportional elements in parallel. The consequence is significantly more actuating effort and the need of better measurement facilities. Lowpass positive definiteness (see Section 5) can eleviate this situation.

1.1 Introductory Examples

1.1.1 Illustration 1. PDT$_2$ System

The PDT$_2$-system

$$G(s) = \frac{s+c}{(s+a)(s+b)} \tag{4}$$

requires $abc > 0$ and $c < a + b$ for positive real part at any frequency ω. This results in the aforementioned case from

$$\Re e\ G(s) = \Re e\ \frac{[\sigma + c + j\omega][\sigma + a - j\omega][\sigma + b - j\omega]}{[(\sigma + a)^2 + \omega^2][(\sigma + b)^2 + \omega^2]}\ . \tag{5}$$

Omitting the imaginary part of the right-hand side and, next, selecting $\sigma = 0$ to obtain the smallest real part, one has

$$\Re e\ G(s) = \frac{(\sigma + a)(\sigma + b)(\sigma + c) + \omega^2(\sigma + a + b - c)}{[(\sigma + a)^2 + \omega^2][(\sigma + b)^2 + \omega^2]} \tag{6}$$

$$= \frac{abc + \omega^2(a + b - c)}{[a^2 + \omega^2][b^2 + \omega^2]}\ . \tag{7}$$

For the sake of illustration, some parameter examples of frequency plots $G(j\omega)$ of stable systems are given in Fig. 1 for $c = 2$. Above the line $a = c - b$, positive realness is satisfied.

Further examples even for unstable (!) ones, where positive realness is not valid, are shown in the Appendix.

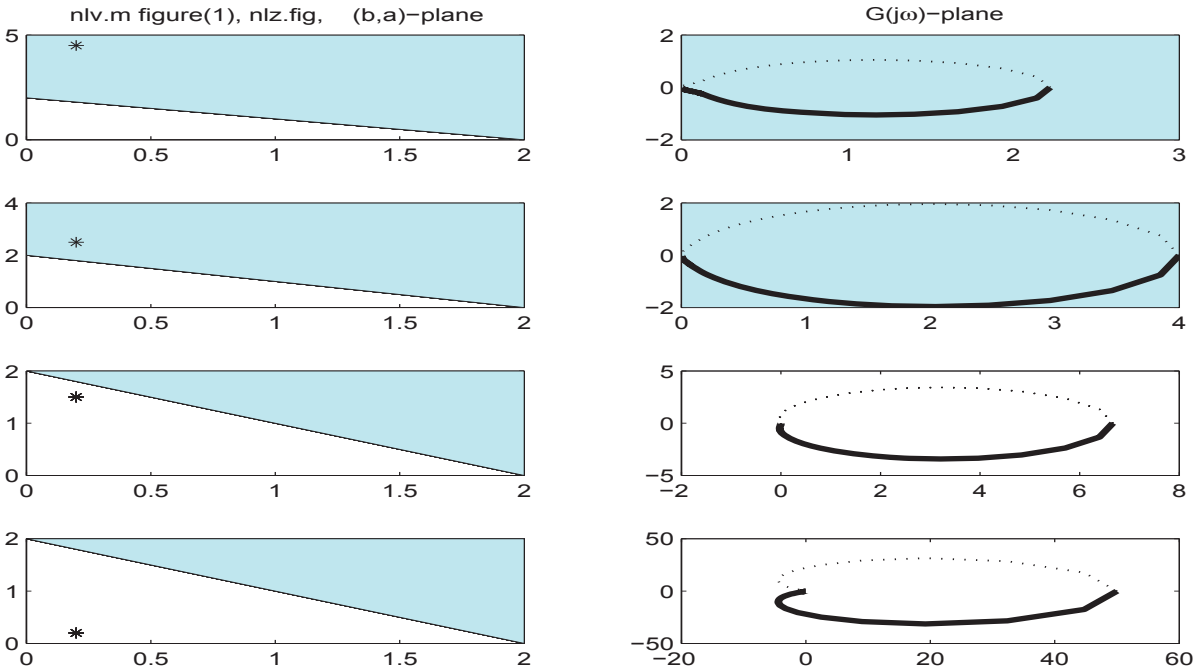

Figure 1: Examples for positive realness and for objecting positive realness

Furthermore, $\Re e\, G(s)$ is displayed in the right-half s-plane (Fig. 2) for some parameters ($a = 0.5;\ b = 1.5;\ c = 4$) where positive realness is not satisfied.The region bound for positive definiteness is given by

$$\omega_0(\sigma) = \sqrt{\frac{(\sigma + a)(\sigma + b)(\sigma + c)}{-\sigma + c - a - b}} \tag{8}$$

and is diplayed by a starred curve.

Multiple parameter changes are better than a single parameter change. Consider initial parameters b and c such that positive realness is not satisfied. Which Δb and Δc of minimum Frobenius norm is required to obtain positive realness? This simple extremum task yields

$$\Delta b^2 + \Delta c^2 + \mu(a + b - c + \Delta b - \Delta c) \quad \rightarrow \min\ . \tag{9}$$

The result is $\Delta c = -\Delta b = \mu/2 = (a + b - c)/2$ with a norm $\Delta b^2 + \Delta c^2 = (a + b - c)^2/2$. If no change of Δb should be admissible the resulting norm is $\Delta c^2 = (a + b - c)^2$, twice the former result.

For the Illustration 1, the Nyquist polar plot plus accompanying plots $G_1(j\omega) = G(\sigma + j\omega)\ \ \forall\ \omega$ for four different values of σ are given in Fig. 5. For $\sigma \neq 0$, G_1 is positive

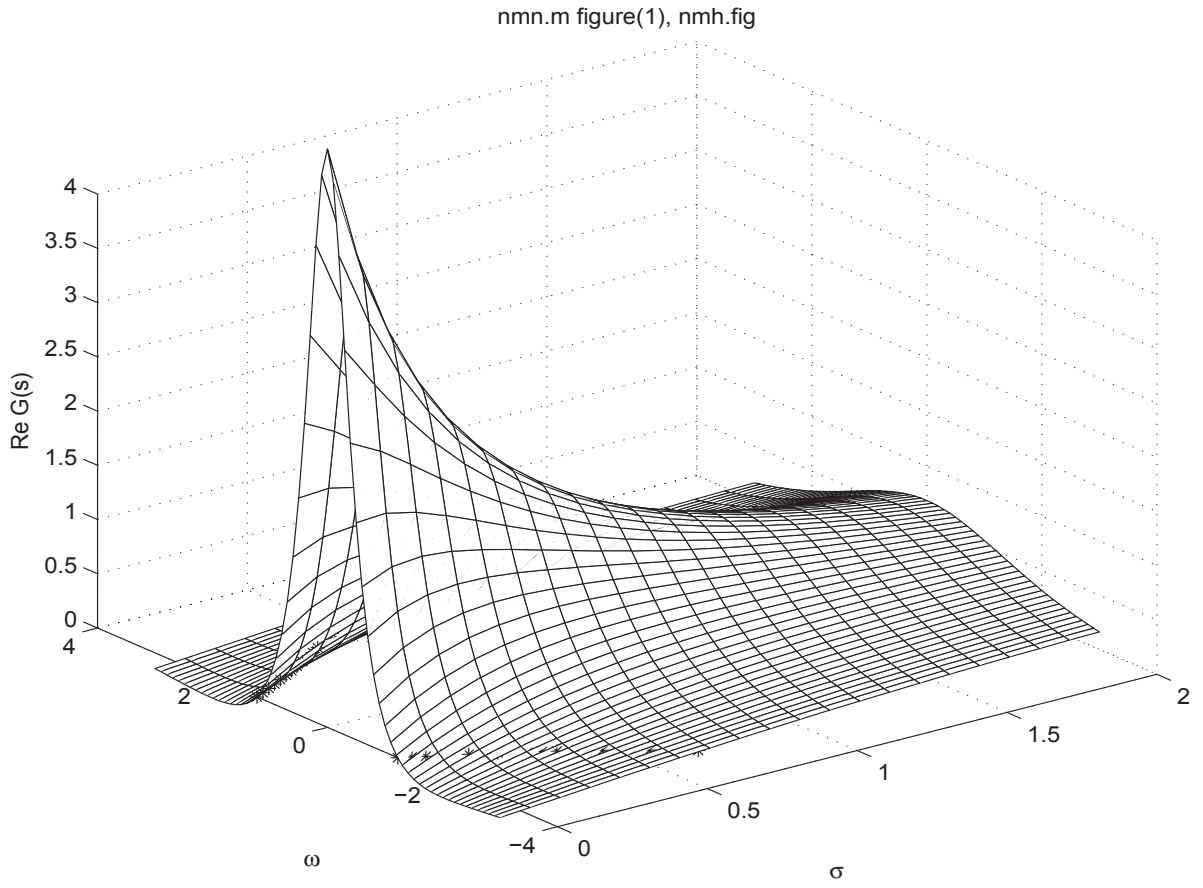

Figure 2: $\Re e\ G(s)$ of Illustration 1 in the right-half s-plane

real for

$$c + \sigma < (a + \sigma) + (b + \sigma) \quad \rightsquigarrow \quad c < a + b + \sigma \ , \tag{10}$$

numerically for $\sigma \geq 1$ and $\omega_0(0)$ referring to Eq.(8). In Fig. 6, the corresponding Nichols charts are given.

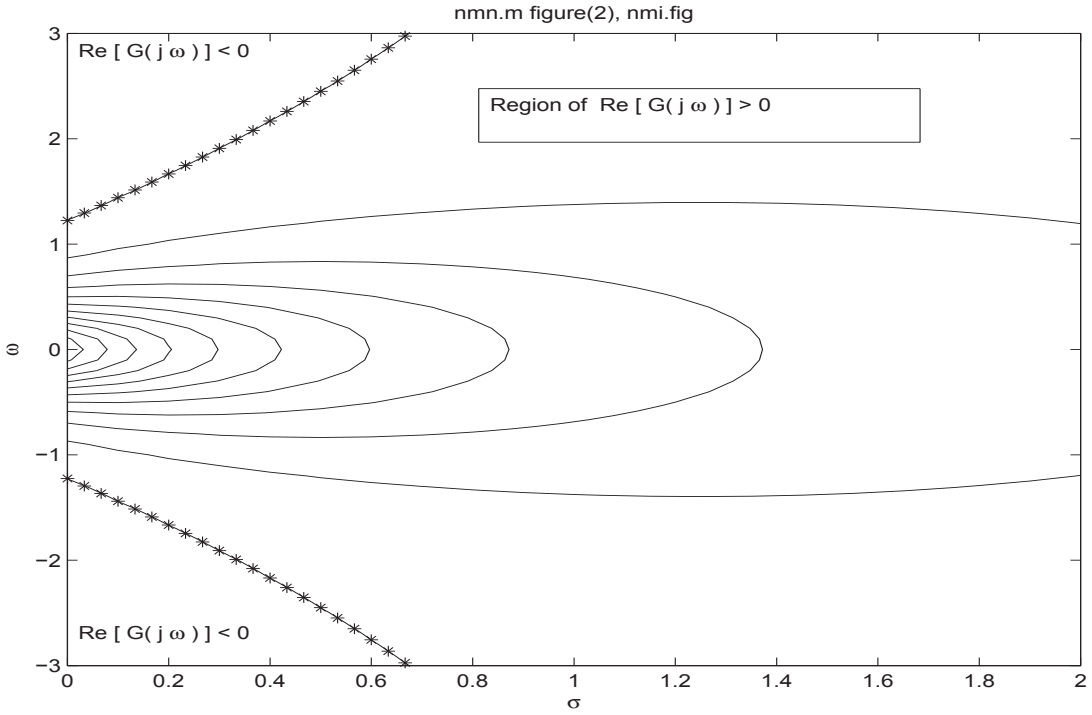

Figure 3: Contour plot of $\Re e\ G(s)$ in the right-half s-plane for Illustration 1

Figure 4: Polar plot of $G(j\omega)$ (Illustration 1)

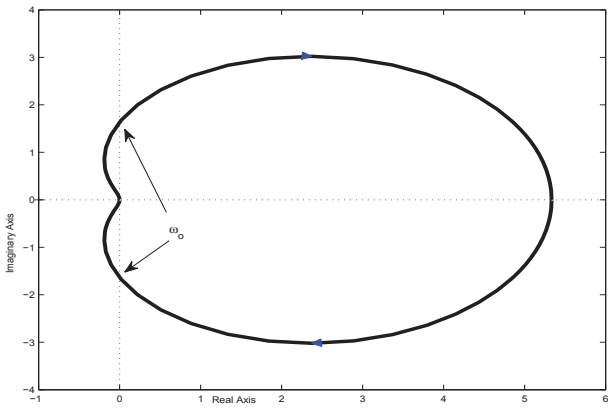

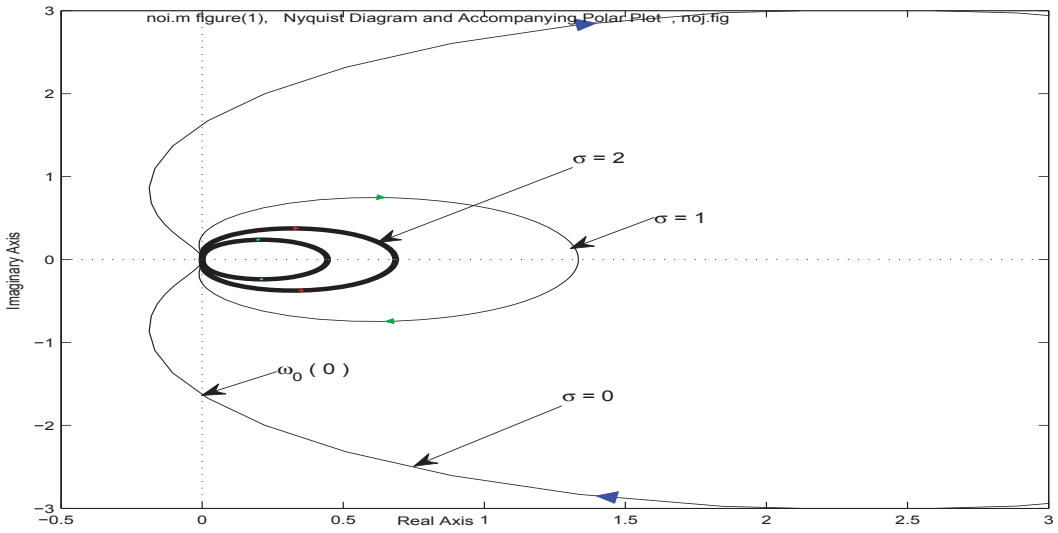

Figure 5: Accompanying plots $G_1(j\omega) = G(\sigma + j\omega)$

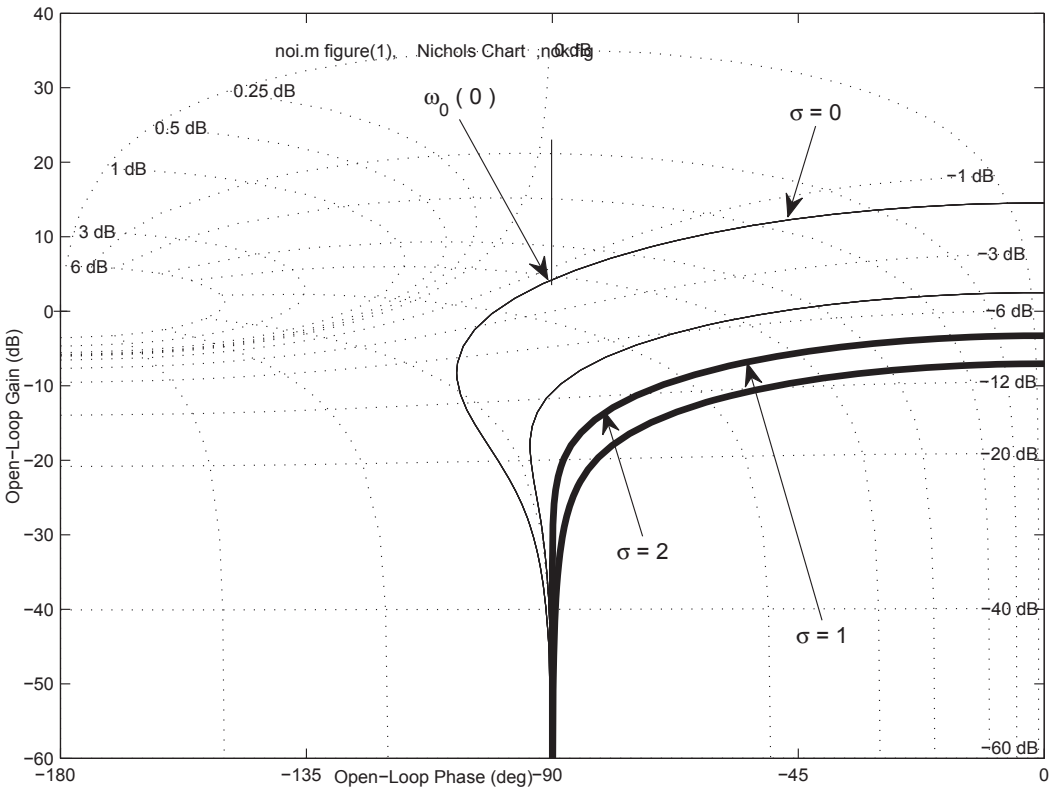

Figure 6: Accompanying Nichols charts for $G_1(j\omega) = G(\sigma + j\omega)$

1.1.2 Example 1. PD_2T_3 System

The PD_2T_3-system

$$G(s) = \frac{(s+c)(s+e)}{(s+a)(s+b)(s+f)} \tag{11}$$

and its $G(j\omega)$ (after having made the denomator real-valued) has a numerator of fifth order

$$(j\omega + c)(j\omega + e)(-j\omega + a)(-j\omega + b)(-j\omega + f), \tag{12}$$

the real-valued part of the corresponding numerator of $G(j\omega)$ is of fourth order; the coefficients of ω^0, ω^2, ω^4 are

$$abcef \triangleq B(1), \tag{13}$$

$$(c+e)(ab+af+bf) - ce(a+b+f) - abf \triangleq B(3), \tag{14}$$

$$a+b-c-e+f \triangleq B(5)\ . \tag{15}$$

2 Coefficients and Conditions for Positive Realness

Via MATLAB and defining a variable A, one finds $B(i)$ for the conditions for positive realness of Example 1, Eq.(11),

```
A=expand((j*om+c)*(j*om+e)*(-j*om+a)*(-j*om+b)*(-j*om+f))
A(1)=A
for i=1:5
    A(i+1)=simplify((A(i)-subs(A(i),om,0))/om); end
for i=1:2:5    % coefficients of om^(i-1): [0  2  4]
    B(i)=subs(A(i),om,0); end
```

Multiplying two general polynomials[1] $a(s)b^*(s)$ (with equal degree up to $n-1$) the coefficients of the powers of ω of the product are given in what follows. The coefficient of ω^{i-1} is

$$\mathrm{tr}[\mathbf{I}_{i\times n}\{(\mathbf{a}\mathbf{b}^T)\ .*\ \mathbf{U}_v\}\mathbf{I}_{i\times n}^T\mathbf{I}_{Ri}] \qquad 1 \le i \le n \tag{16}$$

$$\mathrm{tr}[\mathbf{I}_{(2n-i)\times n}\mathbf{I}_{Rn}\{(\mathbf{a}\mathbf{b}^T)\ .*\ \mathbf{U}_v\}\mathbf{I}_{Rn}^T\mathbf{I}_{(2n-i)\times n}^T\mathbf{I}_{R(2n-i)}] \qquad n+1 \le i \le 2n-1\ , \tag{17}$$

where $.*$ is the dot product and $\mathbf{U}_v$ and $\mathbf{I}_{i\times n}$ are defined by Eqs.(74) and (78), respectively.

[1] equal to the convolution operation which is not available in symbolic operation

Selecting, e.g., degree 3, $n = 4$, one has[2]

```
Product of the polynomial coefficients of
a*bT (vector a times vector b transposed):
   [ a_1*b_1, a_1*b_2, a_1*b_3, a_1*b_4]
   [ a_2*b_1, a_2*b_2, a_2*b_3, a_2*b_4]
   [ a_3*b_1, a_3*b_2, a_3*b_3, a_3*b_4]
   [ a_4*b_1, a_4*b_2, a_4*b_3, a_4*b_4],
after having dot-postmultiplied with matrix U_v, i.e., a*bT .* Uv:
   [    a_1*b_1, -a_1*b_2*i,   -a_1*b_3,  a_1*b_4*i]    i=\sqrt{-1}
   [  a_2*b_1*i,    a_2*b_2, -a_2*b_3*i,   -a_2*b_4]
   [   -a_3*b_1,  a_3*b_2*i,    a_3*b_3, -a_3*b_4*i]
   [ -a_4*b_1*i,   -a_4*b_2,  a_4*b_3*i,    a_4*b_4],
the list of the powers of \omega and the appropriate coefficients:
     0      a_1*b_1
     1      a_2*b_1*i - a_1*b_2*i              i=\sqrt{-1}
     2      a_2*b_2 - a_1*b_3 - a_3*b_1
     3      a_1*b_4*i - a_2*b_3*i + a_3*b_2*i - a_4*b_1*i
     4      a_3*b_3 - a_2*b_4 - a_4*b_2
     5      a_4*b_3*i - a_3*b_4*i
     6      a_4*b_4
```

In cases of differing dimension of $\mathbf{a}$ and $\mathbf{b}$, the smaller vector can be filled up with zeros; or the matrix of the product $\mathbf{ab}^T$ is augmented with rows (columns) of zeros at the bottom (at the right side). The operations carried out in the preceding paragraph can also be handled in cascade if a couple of polynomials are under concern.

Let us remind that the remaining expressions $B(2)$ and $B(4)$ are useful to investigate negative imaginary properties.

2.1 Computer-Assisted Positive Realness

Interested in the conditions for positive realness in the case of controller $K(s)$ and plant $G(s)$, switched in series, one has

$$F_o(s) = \frac{Z_K(s)Z_G(s)}{P_K(s)P_G(s)} = \frac{(\sum_1^n z_{Ki}s^i)(\sum_1^n z_{Gi}s^i)}{(\sum_1^n p_{Ki}s^i)(\sum_1^n p_{Gi}s^i)} \tag{18}$$

$$= \frac{(\mathbf{z}_K^T\mathbf{s})(\mathbf{z}_G^T\mathbf{s})(\mathbf{p}_K^T\mathbf{s}^*)(\mathbf{p}_G^T\mathbf{s}^*)}{(\mathbf{p}_K^T\mathbf{s})(\mathbf{p}_G^T\mathbf{s})(\mathbf{p}_K^T\mathbf{s}^*)(\mathbf{p}_G^T\mathbf{s}^*)} \tag{19}$$

$$= \frac{\mathbf{s}^T(\mathbf{z}_K\mathbf{p}_K^T)\mathbf{S}(\mathbf{z}_G\mathbf{p}_G^T)\mathbf{s}^*}{\mathbf{s}^T(\mathbf{p}_K\mathbf{p}_K^T)\mathbf{S}(\mathbf{p}_G\mathbf{p}_G^T)\mathbf{s}^*} = \frac{\mathbf{s}^T\bar{\mathbf{K}}\mathbf{S}\bar{\mathbf{G}}\mathbf{s}^*}{\mathbf{s}^T\mathbf{P}_K\mathbf{S}\mathbf{P}_G\mathbf{s}^*}\ , \tag{20}$$

[2] We change over to verbatim display, in parts, in order to transmit the impression how the results are presented in original MATLAB

where the following abbreviations have been used

$$\bar{\mathbf{K}} \triangleq \mathbf{z}_K \mathbf{p}_K^T \tag{21}$$
$$\bar{\mathbf{G}} \triangleq \mathbf{z}_G \mathbf{p}_G^T \tag{22}$$
$$\mathbf{P}_K \triangleq \mathbf{p}_K \mathbf{p}_K^T \tag{23}$$
$$\mathbf{P}_G \triangleq \mathbf{p}_G \mathbf{p}_G^T \tag{24}$$
$$\mathbf{s} \triangleq (1 \quad s \quad s^2 \quad \ldots)^T \tag{25}$$
$$\mathbf{s}|_{s=j\omega} = (1 \quad j\omega \quad -\omega^2 \quad \ldots)^T \tag{26}$$
$$\mathbf{s}^*|_{s=j\omega} = (1 \quad -j\omega \quad -\omega^2 \quad \ldots)^T \tag{27}$$
$$\mathbf{S} \triangleq \mathbf{s}^*|_{s=j\omega} \mathbf{s}^T|_{s=j\omega} \ . \tag{28}$$

The scalar expression $\mathbf{s}^T \bar{\mathbf{K}} \mathbf{S} \bar{\mathbf{G}} \mathbf{s}^*|_{s=j\omega} \triangleq A$ is a polynomial of degree $4(n-1)$. The positive realness conditions can be separated by the MATLAB algorithm

```
A(1)=A
for i=1:2*n
    A(i+1)=simplify((A(i)-subs(A(i),om,0))/om); end
for i=1:2:2*n
    B(i)=subs(A(i),om,0); end
```

Since `B(`i`)` is not a valid symbolic variable name, the coefficients of ω^i, which are the basis of the positive realness condition, cannot be denomiated as variables from the very beginning.

3 Permitted Zero Region

Taking into consideration that one is interested in the region for positive definiteness in the (e, c)-plane of Example 1, the signs must be payed special attention. One has

$$B(5) > 0: \quad c + e < a + b + f \tag{29}$$
$$c < (a + b + f) - e \triangleq c_1 \tag{30}$$
$$B(1) > 0: \quad ce > 0 \tag{31}$$
$$c > 0, \qquad e > 0. \tag{32}$$

Condition $B(3)$ is rewritten as

$$c\underbrace{[ab+af+bf-e(a+b+f)]}_{\triangleq p_4}\underbrace{-abf+e(ab+af+bf)}_{\triangleq p_5} > 0 \tag{33}$$

$$cp_4(e)+p_5(e) > 0\ . \tag{34}$$

Depending on the sign, the condition has to be separated. Then, c in relation to the auxiliary quotient $c_2 \triangleq -p_5/p_4$ is

$$p_4>0 \quad : \quad c>-p_5/p_4 \tag{35}$$

$$p_4<0 \quad : \quad c<-p_5/p_4\ . \tag{36}$$

In Fig. 7 the limits are portrayed and the filled area demonstrates the permitted region in the (e,c)-plane.

4 Robustness

In Example 1, we consider the parameters a and b uncertain. The uncertainties Δa and Δb are in an uncertainty box, where $|\Delta a| \le \Delta a_m$ and $\Delta b \le \Delta b_m$. As to be expected, the range of c is reduced, shown in Fig. 8. The result is based on selecting the worst corner of the rectangular uncertainty, only. In order to ascertain that no enclave exists, a huge number of uncertainties inside the rectangle is chosen and the worst result is assigned by a dot line in Fig. 8.

In the vicinity of $e_{crit} = (ab+af+bf)/(a+b+f)$, resulting from $p_4 = 0$, there are numerous opportunities for selecting e in such a constellation. Fortunately, they are excluded by other conditions $B(1)$, $B(5)$, and from physical insight as well.

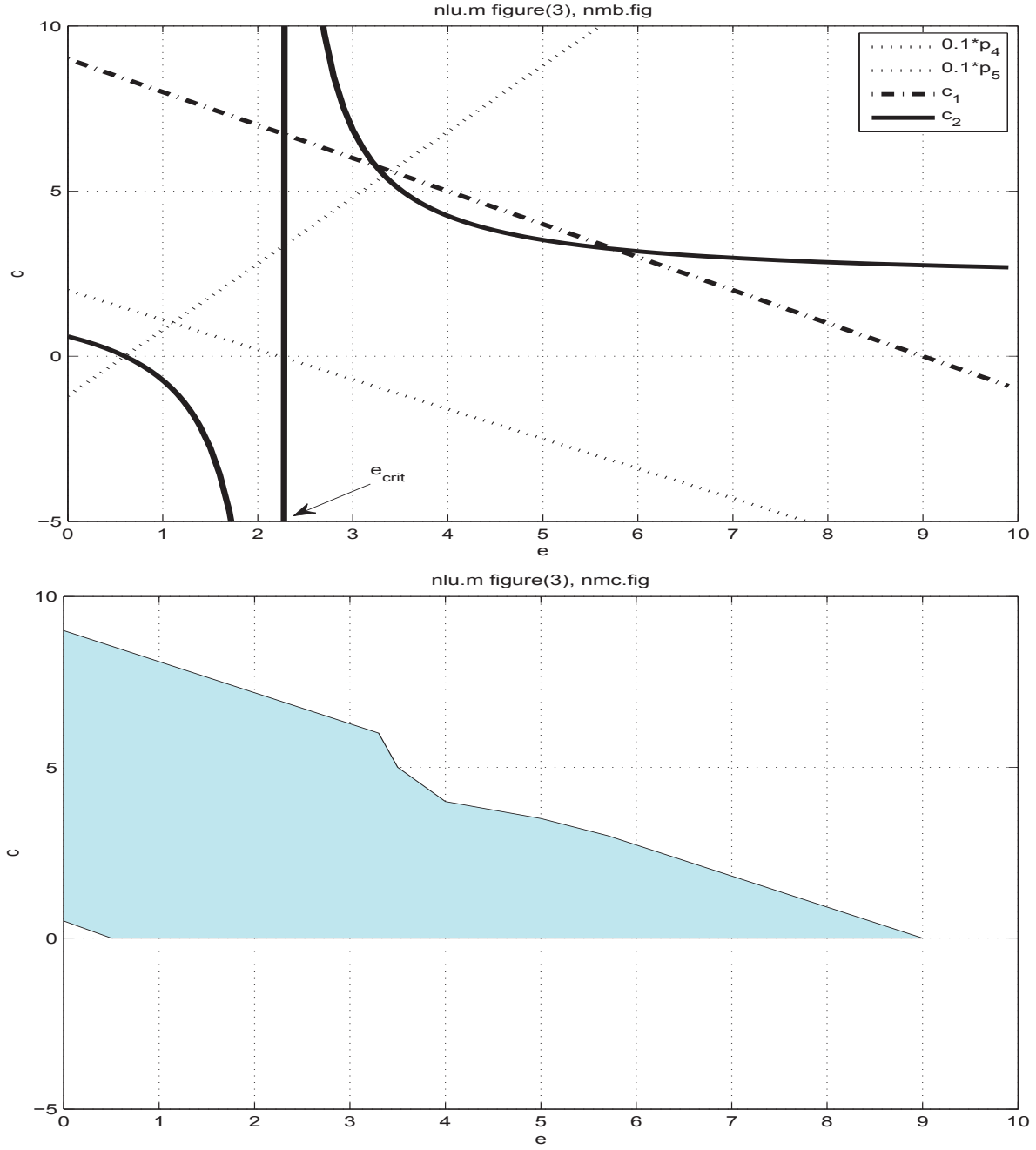

Figure 7: Limits for positive realness for $a = 6;\quad b = 1;\quad f = 2$ (upper part) and Area for permitted values in the (e, c)-plane (lower part) for Example 1

With respect to symmetry one has $c = e$. Investigating the specific point c with maximum tolerable uncertainty in order not to object positive realness, for the Example 1 of Eq.(11) we find from $B(1) > 0$ in Eq.(32) $|\Delta c| \leq c$ or $\Delta c_{\min} = -c$. From $B(5) > 0$ in Eq.(30) results $c < (a+b+f) - e$, $c + \Delta c = (a+b+f)/2 = 4.5$ and $c = 2.25$. From $B(3) > 0$ in Eq.(33) we have

$$(a+b+f)(c+\Delta c)^2 - 2(c+\Delta c)(ab+af+bf) + abf = 0, \tag{37}$$

resulting in $c = \Delta c = 2.06$.

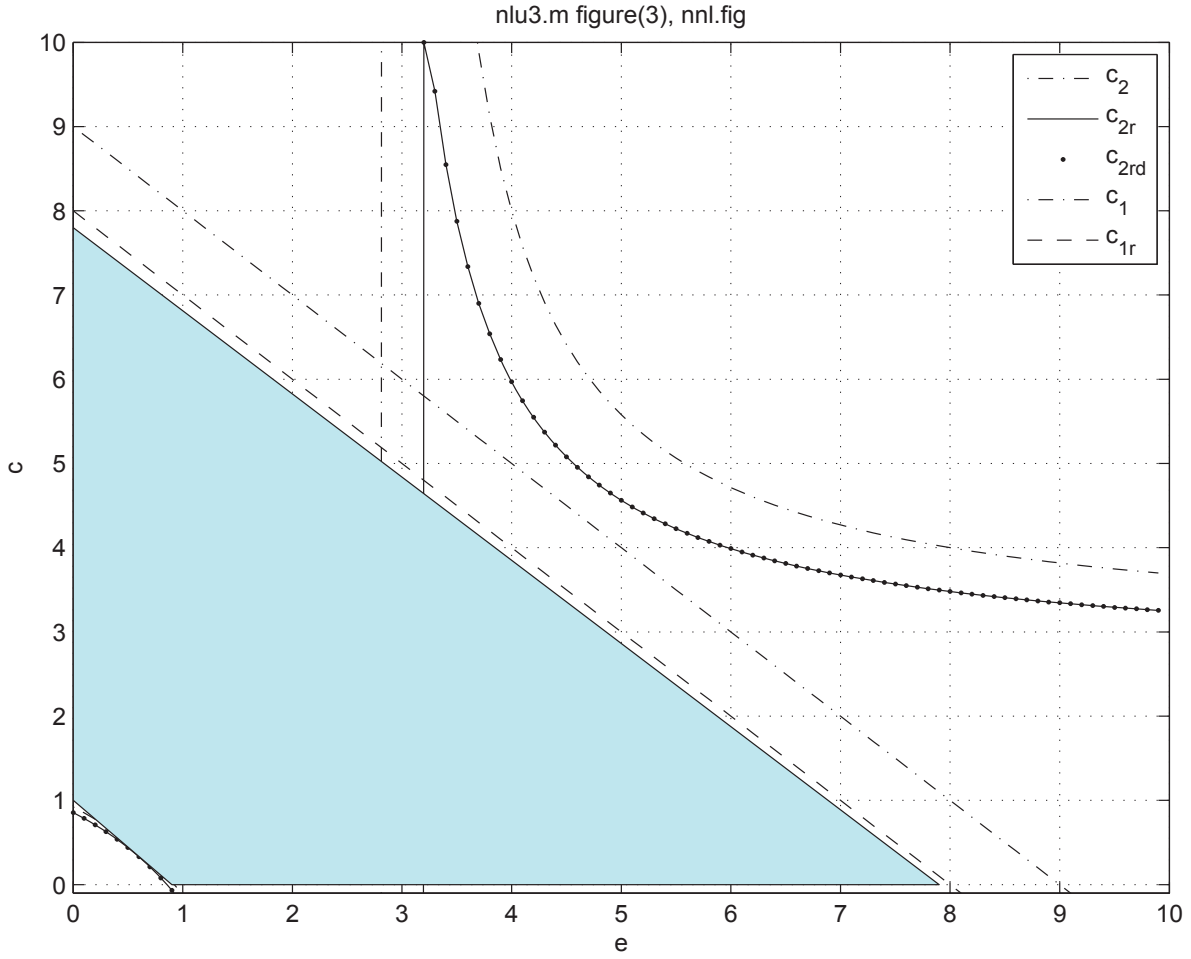

Figure 8: Robust range for positive realness in the case of $a = 4;\ b = 3;\ c = 2;\ \Delta a_m = 0.8;\ \Delta b_m = 0.2$ for Example 1

5 Lowpass Positive Realness

Strictly positive realness offers the advantage: The positive real plant $G(s)$ in combination with an integral contoller $K(s) = 1/(sT_I)$ yields a stable closed-loop system for the region $0 < T_I < \infty$. Stability robustness is guaranteed with respect to any positive T_I.

For some band-limited $G(j\omega)$, i.e.,

$$\Re e\, G(j\omega) > 0 \quad \forall\, \omega < \omega_0\ , \qquad (\text{instead of } \ 0 < \omega < \infty) \tag{38}$$

the value of $\Im m\, G(j\omega_0)$ determines the maximum $|K(j\omega_0)|$ in order not to affect stability, i.e., it suffices to keep Eq.(38) satisfied if the integral controler does not exceed

$$|K(j\omega_0)| < \frac{1}{|\Im m\, G(j\omega_0)|} = \frac{1}{|G(j\omega_0)|}\ . \tag{39}$$

The idea of lowpass positive realness does not work for plants the polar plot of which enters the left half plane at low frequencies, e.g., in the case of the Example 1 of Eq.(11) for $a = 6;\ \ b = 1;\ \ c = 0.1;\ \ e = 0.1;\ \ f = 2$. The corresponding polar plot and the details close to the origin are given in Fig. 9.

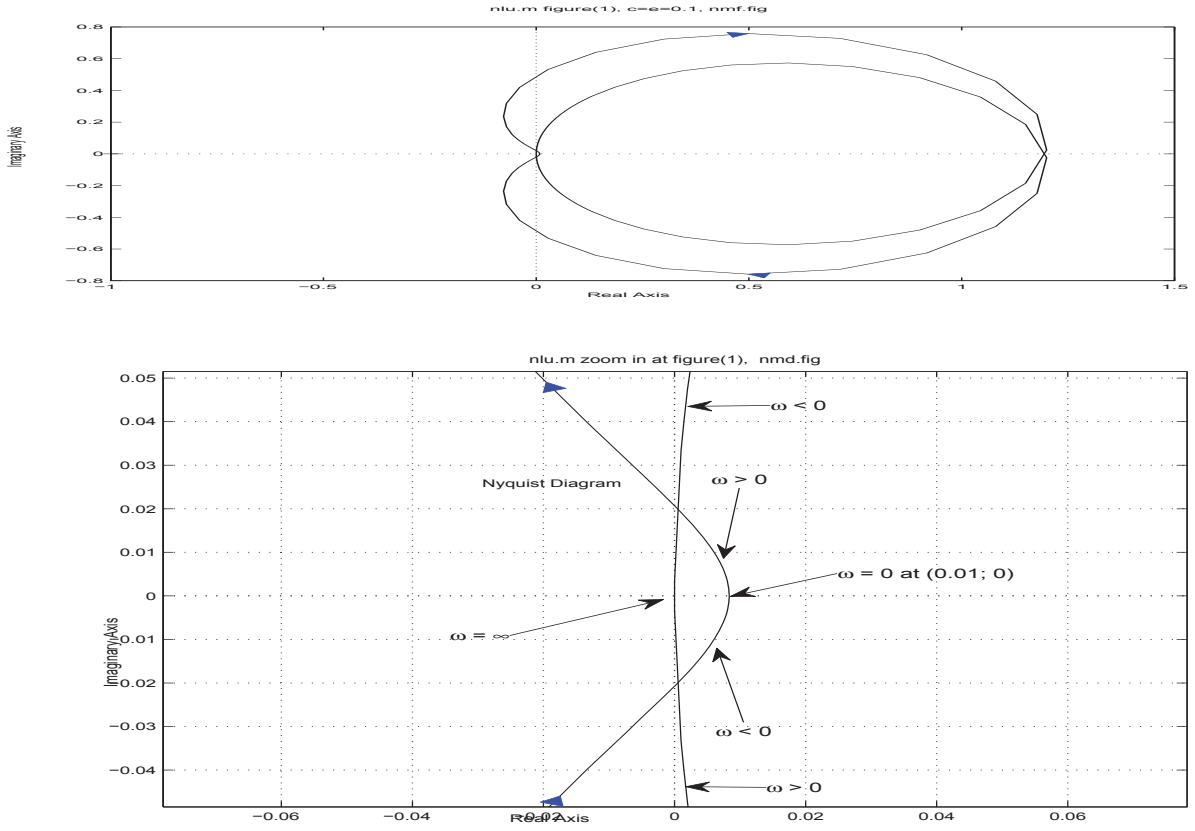

Figure 9: Polar plot for $c = 0.1;\ \ e = 0.1$ and details close to the origin

For the Illustration 1 with the PDT_2-plant, we combine both original conditions $a + b - c > 0$ and $abc > 0$ for the bandwith limit $0 < \omega < \omega_0$ in order to guarantee positive realness in this lowpass region, only,

$$(a + b - c)\omega_0^2 + abc > 0 \tag{40}$$

which results in the larger condition for c

$$c < (a + b)\frac{\omega_0^2}{\omega_0^2 - ab} < a + b \ . \tag{41}$$

For the Example 1 of the PD_2T_3-plant, based on Eq.(15), the combination yields

$$B(1) + B(3)\omega^2 + B(5)\omega^4 \ > \ 0 \tag{42}$$

$$cep_1 + (c + e)p_2 + p_3 \ > \ 0 \ , \tag{43}$$

where

$$p_1 \ \stackrel{\triangle}{=} \ abf - (a + b + f)\omega_0^2 \tag{44}$$

$$p_2 \ \stackrel{\triangle}{=} \ (ab + af + bf)\omega_0^2 - \omega_0^4 \tag{45}$$

$$p_3 \ \stackrel{\triangle}{=} \ -abf\omega_0^2 + (a + b + f)\omega_0^4 \ . \tag{46}$$

The resulting lowpass positive real condition is

$$c > \frac{-(ep_2 + p_3)}{ep_1 + p_2} \quad \forall c_{h2} \stackrel{\triangle}{=} ep_1 + p_2 > 0 \ . \tag{47}$$

Otherwise, the sign of the condition changes, see Fig. 10 upper part.

Fig. 10 demonstates the increase of the area versus Fig. 7.

The gradient of Eq.(43), left-hand side, with respect to c or e is $-p_2/p_1 = 2.66$. The characteristic in Fig. 10 is (c, e)-symmetric.

For $\omega_0 \ \rightarrow \infty$ the result Eq.(47) converges to B(5) in Eq.(15).

Subsequently, there is a combined optimization target

$$\omega_0 + w_1|\Im m \ G(j\omega_0)| \rightarrow \text{opt} \ \ \text{s.t.} \ \ \Re e \ G(j\omega) > 0 \ \ \forall \ \omega < \omega_0 \ , \tag{48}$$

in order to obtain, e.g., $|K(j\omega_0)| \rightarrow \min$, see Eq.(58). The condition with the Frobenius norm $\|(\Delta a \ \vdots \ \Delta b)\|_F^2 < d_o$ can be included via Lagrange multiplier.

In addition, lowpass positive realness does not require degree difference 1 or lower. Higher difference is permitted. E.g., replacing the numerator in Eq.(4) by a constant, positive realness is satisfied for $\omega < \omega_0 = \sqrt{ab}$.

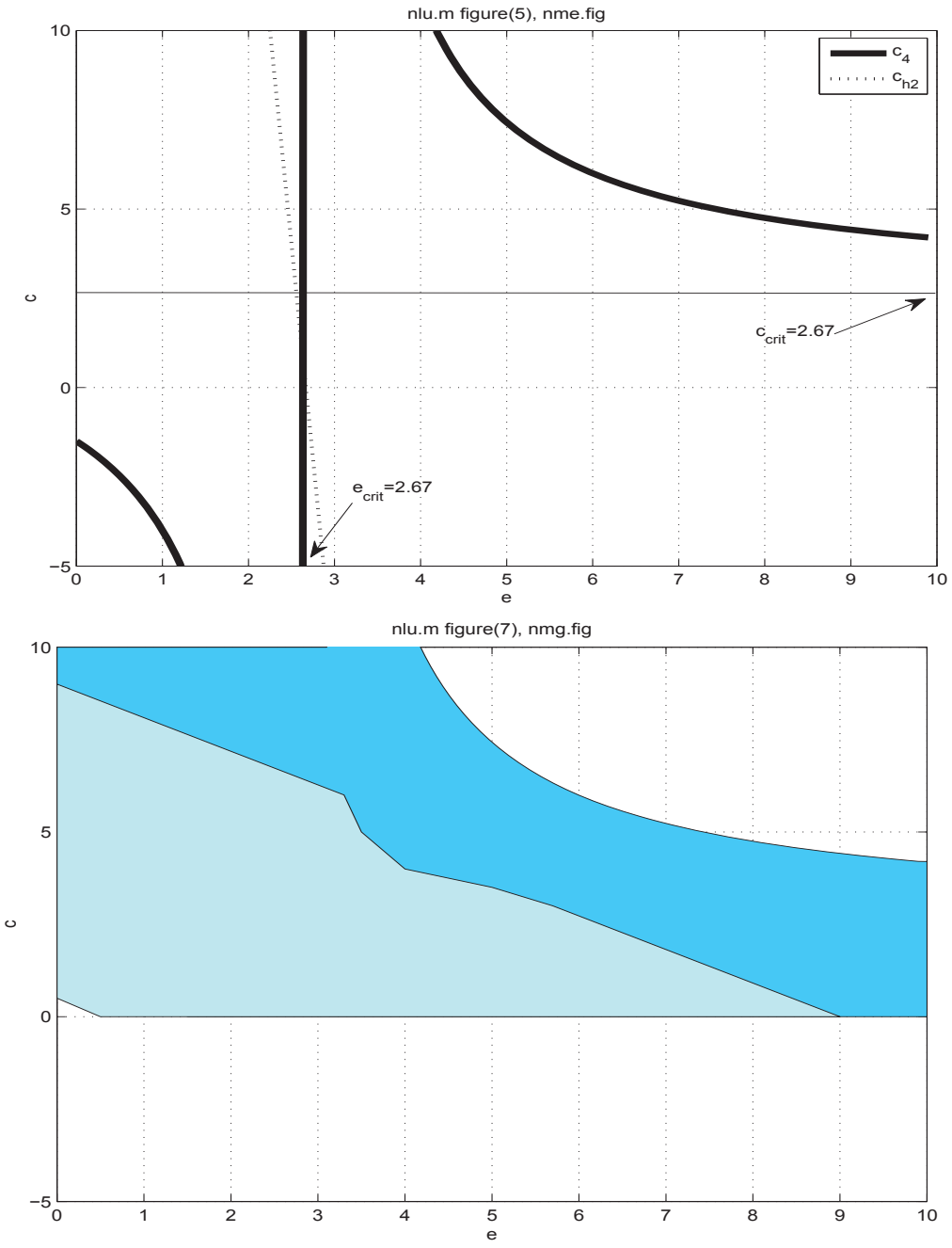

Figure 10: Lowpass positive realness conditions for $\omega_0 = 2, \quad a = 6, \quad b = 1, \quad f = 2$ (upper part) and Lowpass positive realness area (lower part) including the results given in Fig. 7 for comparison

6 Gradients to Approach Positive Realness

6.1 Changing Parameters

Consider the parameters $c,\ e$ alterable. Find the gradients such that the nonpositive conditions $B(i)$ are changed in order to obtain a positive definite function. Only the nonpositive conditions should be changed. Hence, a weight $\mathbf{v}$ is defined, a component of which is 1 in case of necessary change and 0 in case after having arrived at positive definiteness. Thus,

$$\mathbf{v} \stackrel{\triangle}{=} 0.5\mathrm{vec}_i\{[1 - B(i)/|B(i)|]w_i\}, \tag{49}$$

where w_i weights the various condition gradients. Then, $v_i = 0$ for $B(i) > 0$ and $v_i = 1$ for $B(i) < 0$. Defining

$$\mathbf{k} \stackrel{\triangle}{=} (c \quad e)^T \tag{50}$$

$$\mathbf{h} \stackrel{\triangle}{=} \mathrm{vec}_i[B(i)] \tag{51}$$

the affordable changes $\Delta c,\ \Delta e$ result from the gradient, the weighting vector $\mathbf{v}$ applied to each gradient element and the stepsize Δr

$$\Delta\mathbf{k} = \begin{pmatrix}\Delta c\\ \Delta e\end{pmatrix} = (\frac{\partial \mathbf{h}^T}{\partial \mathbf{k}})\ \mathbf{v}\ \Delta r = \begin{pmatrix} \frac{\partial h_1}{\partial c} & \frac{\partial h_1}{\partial e} \\ \frac{\partial h_2}{\partial c} & \frac{\partial h_2}{\partial e} \\ \frac{\partial h_3}{\partial c} & \frac{\partial h_3}{\partial e} \end{pmatrix}^T \mathbf{v}\ \Delta r\ . \tag{52}$$

The Jacobi matrix elements are calculated by symbolic differentiation. In the numerical Illustration 1 with data of Fig. 7, the result is depicted in Fig. 11.

6.2 Changes of the Limit Frequency

Now, find the sensitivity of ω_0 with respect to a selected parameter a_j in $G(j\omega)$. We abbreviate the general case with order n, as demonstrated in Eq.(7) for $n = 2$,

$$\Re e\ G(j\omega) \stackrel{\triangle}{=} \frac{\sum_{i=0,2,4,\ldots}^{n} g_i\ \omega_0^i}{N(\omega)}\ . \tag{53}$$

Denoting $\omega = \omega_0$ at $\Re e\ G(j\omega) = 0$ yields

$$\sum_{i=0,2,4,\ldots}^{n} g_i\ \omega_0^i = 0\ . \tag{54}$$

An infinitesimally small deviation Δa_j of any parameter is supposed to trigger a deviation $\Delta\omega_0$ of the limit frequency ω_0. Hence,

$$\frac{\partial \sum_{i=0,2,4,\ldots}^{n} g_i\ \omega_0^i}{\partial a_j} = \sum_{i=0,2,4,\ldots}^{n} \frac{\partial g_i}{\partial a_j}\omega_0^i + [\sum_{i=0,2,4,\ldots}^{n} i\ g_i\ \omega_0^{i-1}]\frac{\partial \omega_0}{\partial a_j} = 0\ . \tag{55}$$

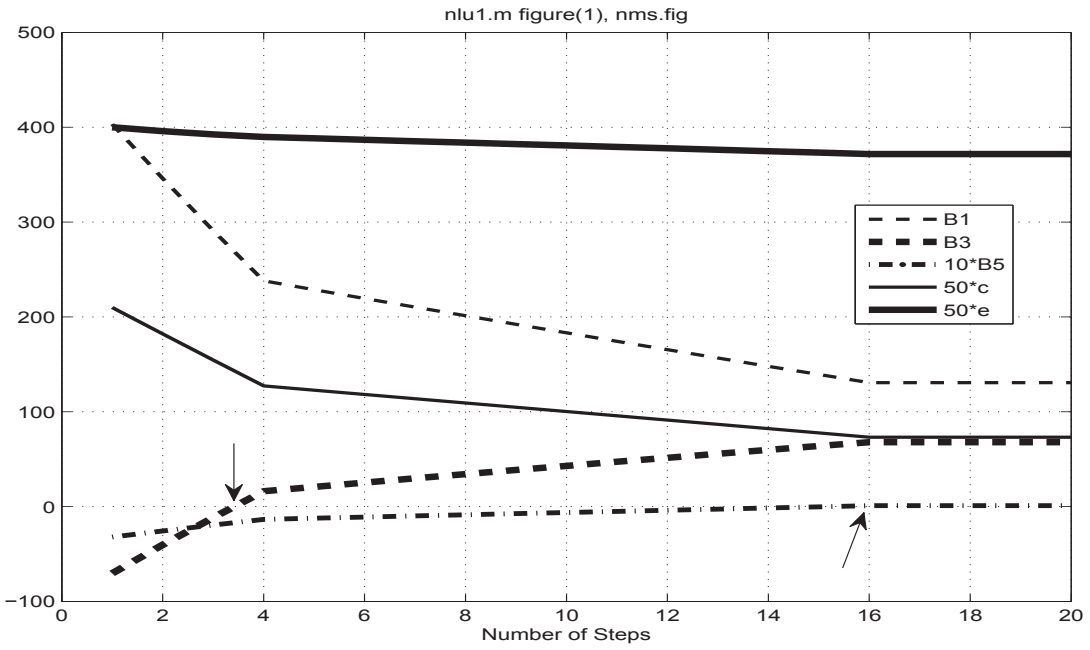

Figure 11: Approaching positive definiteness via gradient method. The arrows denote the zero crossover

Finally, one has

$$\frac{\partial \omega_0}{\partial a_j} = -\frac{\sum_{i=0,2,4,\ldots}^{n} \frac{\partial g_i}{\partial a_j}^{\,i}}{\omega_0^{\,i}} \sum_{i=2,4,\ldots}^{n} i\ \omega_0^{i-1}\ g_i\ . \tag{56}$$

For the Illustration 1 with Eq.(4), we find $\omega_0 = \sqrt{abc/(c-a-b)}$ and

$$\frac{\partial \omega_0}{\partial c} = \frac{ab - \omega_0^2}{2\omega_0(c-a-b)} \tag{57}$$

and Fig. 12.

6.3 Changes of the Imaginary Part at the Limit Frequency

For the control system with integral controller $K = 1/(j\omega T_I)$, the plant G and the gain margin A_R , one has

$$A_R K G = 1 \quad \rightsquigarrow \quad \frac{A_R}{T_I} = \frac{\omega_0}{|\Im m\ G(j\omega_0)|}\ . \tag{58}$$

Pay attention to the property that moving the zero c towards the origin the gain margin A_R can be increased referring to both ω_0 and $\Im m\ G(j\omega_0)$, see Fig. 12.

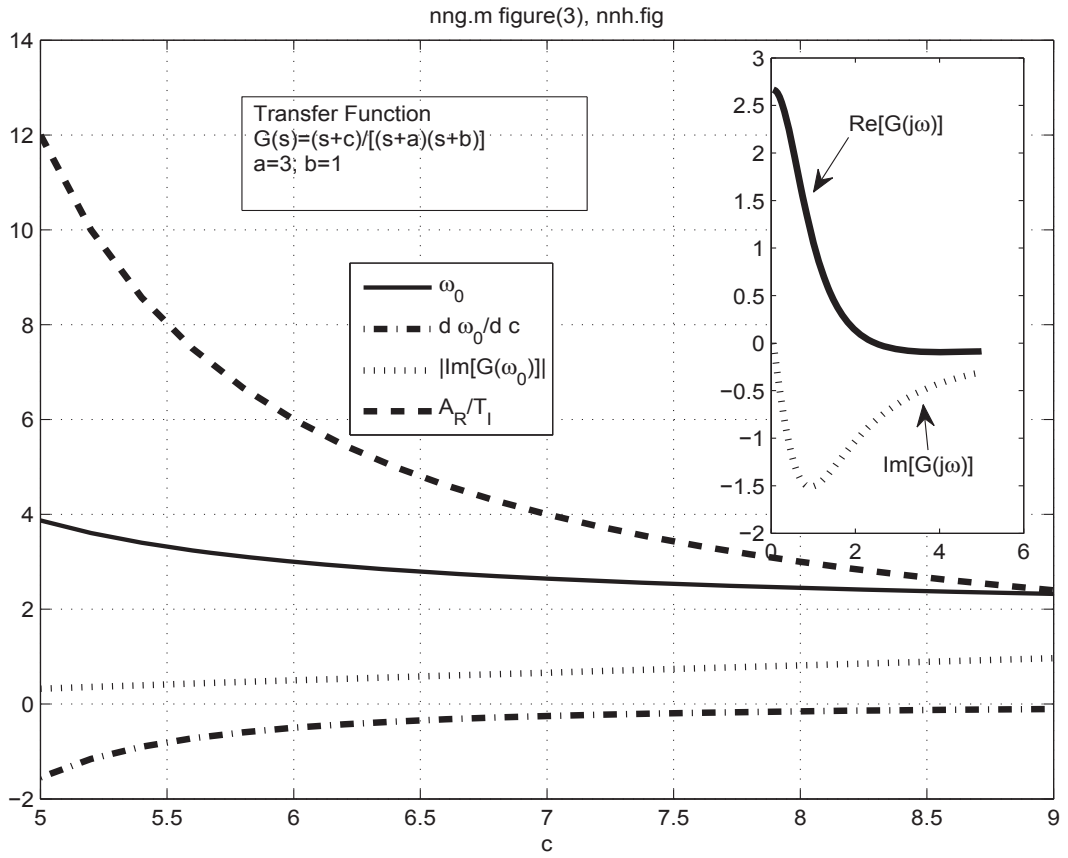

Figure 12: Influence of the zero c upon closed-loop properties for the Illustration 1

The dependence of $\Im m\ G(j\omega_0)$ on any parameter a_j easily results from

$$\frac{\partial \Im m\ G(j\omega_0)}{\partial a_j} = \frac{\partial \Im m\ z(j\omega_0)n^*(j\omega_0)}{\partial a_j}\frac{1}{n(j\omega_0)n^*(j\omega_0)} - [\Im m\ z(j\omega_0)n^*(j\omega_0)]\frac{1}{[n(j\omega_0)n^*(j\omega_0)]^2}\frac{\partial n(j\omega_0)n^*(j\omega_0)}{\partial a_j}, \quad (59)$$

where $n(j\omega_0)$ and $z(j\omega_0)$ are the numerator and the denominator polynomial of $G(j\omega_0)$, respectively.

7 Optimizing Lowpass Realness and Integral Controller

For the Example 1 of Eq.(11), find the tradeoff between large ω_0 and big factor T_I of the integral controller, both in the presence of a given gain margin A_R. Some increase in ω_0 can be considered as a reserve for robustness versus unstructured uncertainty or unknown

high-frequency dynamics. Following Eq.(58)

$$d_m(c) \stackrel{\triangle}{=} 1/\omega_0 + w_1\omega_0/|\Im m\ [G(j\omega_0)]| \quad \rightarrow \quad \min_c\ , \tag{60}$$

where

$$\omega_0 = \sqrt{abc/(c-a-b)}, \quad c > a+b, \quad \Im m\ G(j\omega) = -\omega\frac{\omega^2 + c(a+b) - ab}{(\omega^2+a^2)(\omega^2+b^2)}\ , \tag{61}$$

the result is illustrated in Fig. 13.

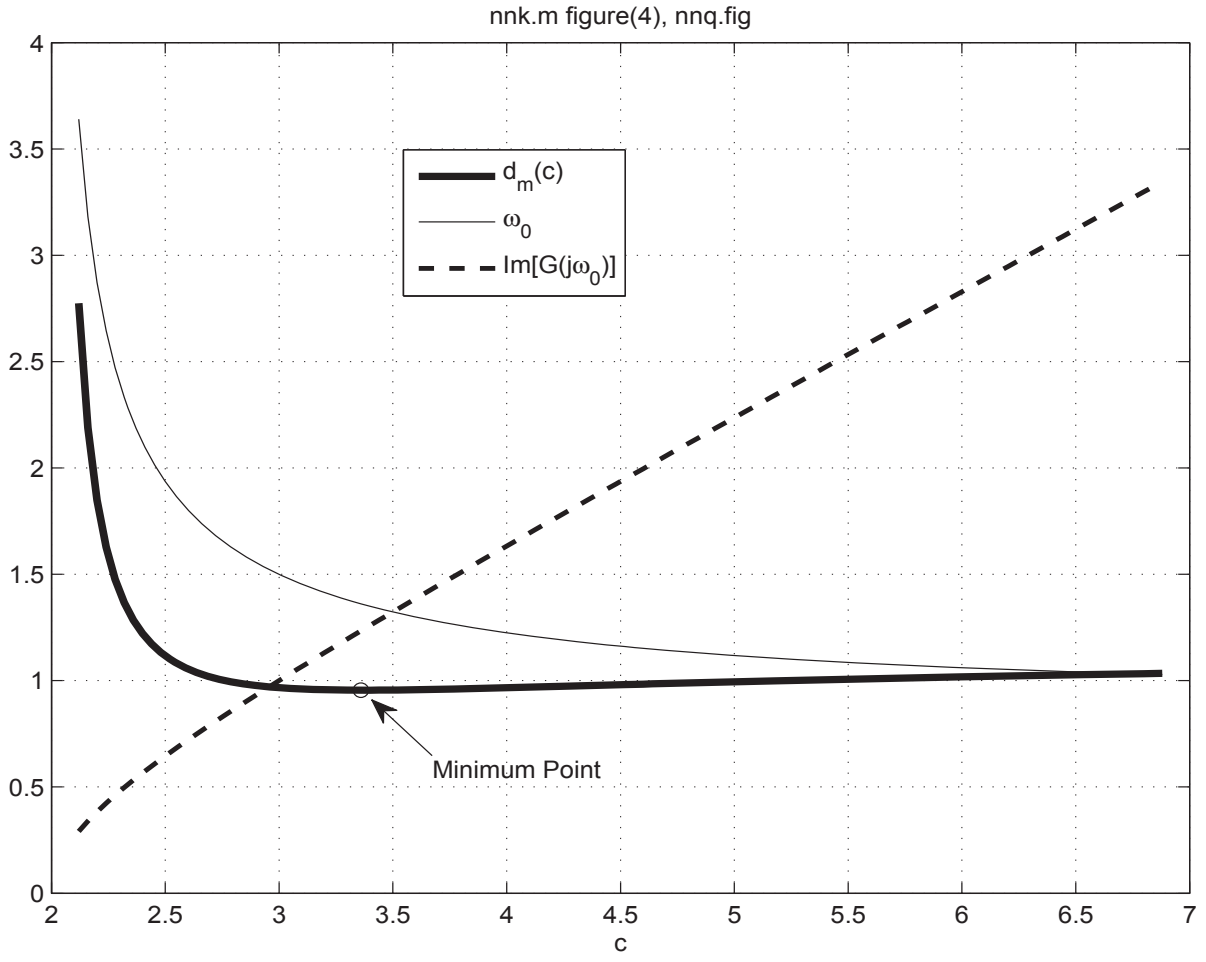

Figure 13: Optimizing ω_0 and T_I versus c

8 Hyperstability Requirements

A multivariable dynamical system in state-space representation

$$\dot{\mathbf{x}}(t) = \mathbf{A}\mathbf{x}(t) + \mathbf{B}\mathbf{u}(t), \qquad \mathbf{x}(0) = \mathbf{x}_o \tag{62}$$

$$\mathbf{y}(t) = \mathbf{C}\mathbf{x}(t) \tag{63}$$

is hyperstable (asymptotically hyperstable) if the transfer matrix $\mathbf{G}(s)$ is positive real (strictly positive) real, where

$$\mathbf{G}(s) = \mathbf{C}(s\mathbf{I} - \mathbf{A})^{-1}\mathbf{B} + \mathbf{D} = \left[\begin{array}{c|c} \mathbf{A} & \mathbf{B} \\ \hline \mathbf{C} & \mathbf{D} \end{array}\right] . \tag{64}$$

Following Kalman Yakubovich (*Slotine, J.J., and Weiping, Li, 1991*), a controllable and observable continuous-time LTI system with m inputs and outputs is hyperstable if there exist symmetric and positive definite matrices $\mathbf{P}$, $\mathbf{L}$ und $\mathbf{V}$ and the following equations

$$\mathbf{A}^T\mathbf{P} + \mathbf{P}\mathbf{A} = -\mathbf{L}\mathbf{L}^T \tag{65}$$

$$\mathbf{C}^T - \mathbf{P}\mathbf{B} = \mathbf{L}\mathbf{V} \tag{66}$$

$$\mathbf{D} + \mathbf{D}^T = \mathbf{V}^T\mathbf{V} \tag{67}$$

are satisfied, where ($\mathbf{A},\ \mathbf{P} \in \mathcal{R}^{n\times n},\ \mathbf{L} \in \mathcal{R}^{n\times l},\ \mathbf{V} \in \mathcal{R}^{l\times m}, \mathbf{C} \in \mathcal{R}^{m\times n}\ , \mathbf{B} \in \mathcal{R}^{n\times m}$). If $\mathbf{L}$ is row regular then the system is asymptotically hyperstable. (A matrix $\mathbf{L}$ is row regular if $\mathbf{L}^T\mathbf{x} = \mathbf{0}$ is only possible for $\mathbf{x} = \mathbf{0}$.) The matrices $\mathbf{L}$ and $\mathbf{V}$ are arbitrary, $\mathbf{P}$ must be positive definite.

[For a discrete-time system, the conditions are

$$\mathbf{\Phi}^T\mathbf{P}\mathbf{\Phi} - \mathbf{P} = -\mathbf{L}\mathbf{L}^T \quad \text{where} \quad \mathbf{\Phi} = \mathbf{\Phi}(T) = e^{\mathbf{A}T} \tag{68}$$

$$\mathbf{C}^T - \mathbf{A}^T\mathbf{P}\mathbf{\Psi} = \mathbf{L}\mathbf{V} \tag{69}$$

$$\mathbf{D} + \mathbf{D}^T - \mathbf{\Psi}^T\mathbf{P}\mathbf{\Psi} = \mathbf{V}^T\mathbf{V}\ .] \tag{70}$$

To impose a system positive definiteness, we remind (for $\mathbf{D}^T = \mathbf{D}$) the artificial algebraic transit matrix $\tilde{\mathbf{D}}$

$$\tilde{\mathbf{D}} \triangleq 0.5\mathbf{V}^T\mathbf{V} - \mathbf{D} = -0.5(\mathbf{C} - \mathbf{B}^T\mathbf{P}^T)\ \mathbf{L}^{-T}\mathbf{L}^{-1}\ (\mathbf{C}^T - \mathbf{P}\mathbf{B})\ . \tag{71}$$

Then the control system obeys the algebraic transit matrix $0.5\mathbf{V}^T\mathbf{V}$.

If positive definiteness is not satisfied yet then find an increment of $\mathbf{L}$ in order to improve positive definiteness of $\mathbf{P}$ via gradients of the northwest subdeterminants of $\mathbf{P}$.

See Eq.(80). That is, evaluate the northwest subdeterminants d_i of $\mathbf{P}$, select the smallest one, which usually might be negative. Then calculate the differential quotient and the increment $\Delta\mathbf{L}$

$$\frac{\partial \min d_i}{\partial \mathbf{L}} \ , \qquad \Delta\mathbf{L} \propto \frac{\partial \min d_i}{\partial \mathbf{L}} = \kappa \ \frac{\partial \min d_i}{\partial \mathbf{L}} \ . \tag{72}$$

Numerically, the differential quotient is determined as the difference quotient

$$\frac{\partial \min d_i}{\partial \mathbf{L}} = \mathrm{matrix}_{kj}[\frac{d_{\min}(\mathbf{L} + \Delta L_{kj}) - d_{\min}(\mathbf{L})}{\Delta L_{kj}}] \ . \tag{73}$$

The gradient increment is executed repeatedly until all the negative d_i have been nearly diminished, see the Example 2 in what follows. Numerical applications may require very small ΔL_{kj} in order not to skip to singular a matrix $\mathbf{L}$. In such a way, positive definiteness can only be approached; a breakthrough to definitively positive definte matrices is not possible for small increments.

8.1 Example 2: Gradients to Approach Positive Definiteness

The example which follows demostrates the procedure of turning all $d_i \ \rightarrow 0$; even though the consequence of this action is $\det \mathbf{P} = 0$. Hence, $\mathbf{P}$ becomes singular and not positive definite. The example is of formal utility, only, applicable in automatic control as an example for a necessary condition for positive realness. Fig. 14 illustrates this minimum search. The quantity $\min d_i$ is depicted versus search step number. The inserted subplot shows the switch of i from $\arg[\min(d_i)]$ from $i = 1$ to $i = 2$ at step number 10.

```
                -15.8745    0.1285    1.4106    4.8886
      A =         7.9216  -16.1339    7.3222    9.7139
                  1.4544    4.8523  -11.0893    1.1245
                  4.8914    8.3823    0.3449  -10.5679

  initial L=diag(abs(rand(n,1)))=                    final Lv =
 0.6385    0         0         0              0.6107  -0.0520  -0.0341  -0.0631
 0    0.5942         0         0             -0.0690   0.3540  -0.1184  -0.2094
 0         0    0.4986         0             -0.0463  -0.1279   0.4341  -0.1170
 0         0         0    0.5679             -0.0822  -0.2164  -0.1117   0.3686
   min d= -0.2317                              min dv= -1.9 e-007
                 P=                                        Pv=
-0.2317  -0.2390  -0.1980  -0.3476           0.0086  -0.0036  -0.0035  -0.0041
-0.2390  -0.2265  -0.1931  -0.3415          -0.0036   0.0016  -0.0033  -0.0062
-0.1980  -0.1931  -0.1504  -0.2850          -0.0035  -0.0033   0.0071  -0.0070
-0.3476  -0.3415  -0.2850  -0.4898          -0.0041  -0.0062  -0.0070   0.0012
                 d=                                      dv=
-0.2317  -0.0047  -0.0001  -0.0000           0.0086   0.0000  -0.0000  -0.0000
```

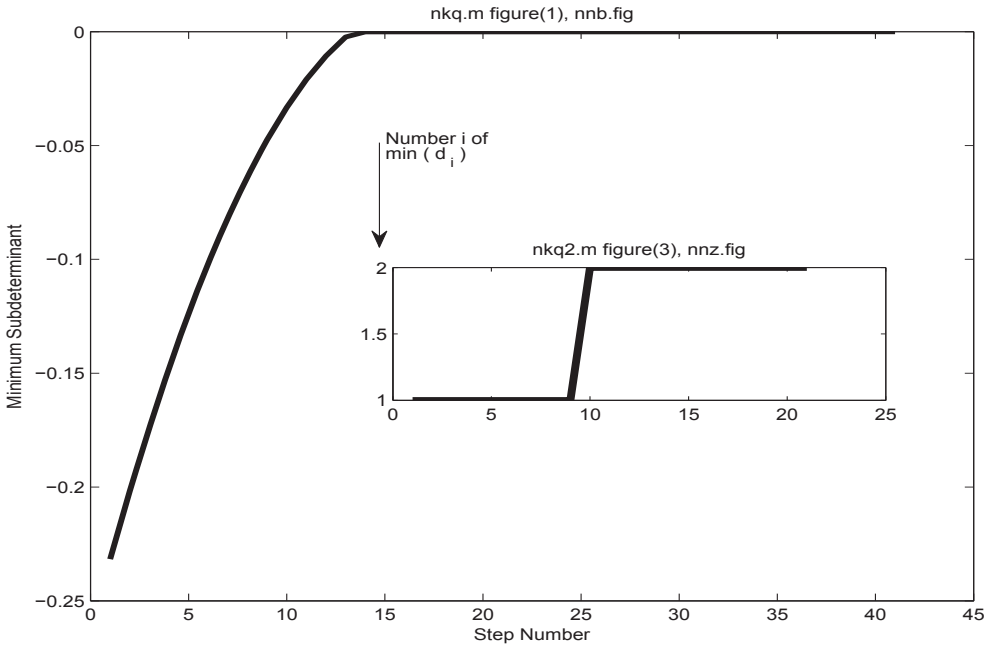

Figure 14: The minimum of all the d_i during minimum search (Example 2)

8.2 Example 3: Gradients to Enter Positive Definiteness

This Example 3 highlights the zero crossover for the negative subdeterminant and their increase when following the gradient procedure.

```
                  -3.6291    1.3402    0.1793   -0.3948
           Ao =    0.7605   -0.8343    0.9134   -0.0899
                   0.7092    3.4872   -3.6918   -1.6077
                   2.1363    8.2571    0.9414  -10.2354
  initial L=diag(abs(rand(n,1)))=                  final Lv =
 0.6380    0         0         0              0.6676  0.0234  0.0235  0.0244
 0    0.5940         0         0              0.0233  0.6214  0.0233  0.0264
 0         0    0.4980         0              0.0236  0.0236  0.5300  0.0252
 0         0         0    0.5679              0.0247  0.0269  0.0251  0.6014
   min d= -0.2265                             min dv= 1.07 e-004
                P=                                          Pv=
-0.2265  -0.2339  -0.1939  -0.3404            0.2252  0.7127  0.1823 -0.0363
-0.2339  -0.2215  -0.1891  -0.3344            0.7127  3.0283  0.7626 -0.1553
-0.1939  -0.1891  -0.1471  -0.2793            0.1823  0.7626  0.2249 -0.0427
-0.3404  -0.3344  -0.2793  -0.4796           -0.0363 -0.1553 -0.0427  0.0272
                d=                                          dv=
-0.2265  -0.0045  -0.0001  -0.0000            0.2252  0.1741  0.0057  0.0001
```

9 Conclusion

Positive realness is extended for application-oriented purposes. The regions of positive realness are investigated in the parameter plane. In the presence of parameter uncertainties, the realness conditions are studied in order to develop robust algorithms, and to extend positive realness in a predetermined lowpass frequency region. Furthermore, gradients are given to approach positive realness conditions for applications with arbitrary partly alterable data.

Eventually, positive definiteness of a matrix is effected by using gradients with respect to an auxiliary matrix, which influences especially the worst subdeterminant of the matrix. This method is used in the field of Lyapunov stability and hyperstability.

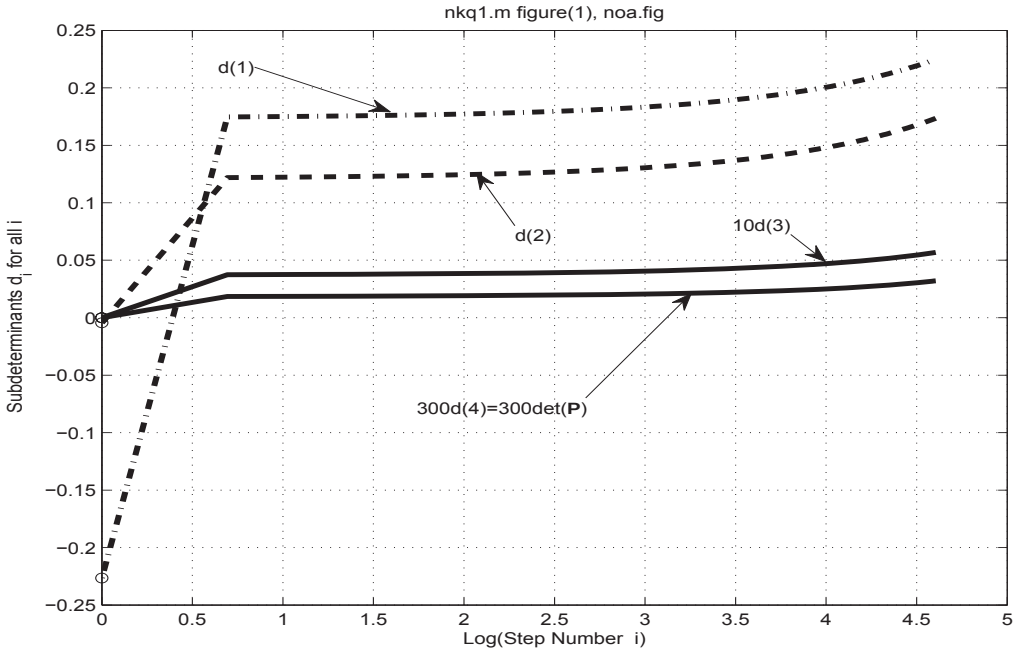

Figure 15: Subdeterminants d_i (with different scale) during the search process in Example 3

References

Adamy, J., 2009, Nichtlineare Regelungen, Berlin: Springer-Verlag

Föllinger, O., 1993, Nichtlinear Regelungen, München: Oldenbourg-Verlag

Kalman, R.E., and Bertram, J.E., 1960, Control system analysis and design via the ßecond methodöf Lyapunov *Trans. ASME - Series D - J. of Basic Engineering* **82**, pp. 371-400

Ljung, L., 1977, On positive real transfer functions and the convergence of some recursive schemes, *IEEE-Trans.* **AC-22**, pp. 539-551

Lozano-Leal, R., and Joshi, S.M., 1990, Strictly positive real transfer functions revisited, *IEEE-Trans.* **AC-35**, pp. 1243-1245

Marquez, H.J., and Damaren, C.J., 1996, Analysis and synthesis of strictly positive real transfer functions, *J. Franklin Inst.* **333(B)**, No. 2, pp. 245-256

Ostertag, E., 2010, Mono- and multivariable control and estimation. Linear, quadratic and LMI methods, Berlin: Springer-Verlag.

Petersen, I.R., and Lanzon, A., 2010, Feedback control of negative-imaginary systems, *IEEE Control Systems Magazine* **30**, No. 5, pp. 54-72

Slotine, J.J., and Weiping, Li, 1991, Applied nonlinear control. Englewood Cliffs:

Prentice-Hall.

NN, Nonlinear systems and control lecture No. 15, Positive real transfer function and connection with Lyapunov Stability, http://www.egr.msu.edu/ khalil/NonlinearSystems/Sample/Lect15.pdf

NN, Positve-definite function. From Wikipedia, the free encyclopedia http://en.wikipedia.org/wiki/Positive_definite_function

NN, Positive real functions https://ccrma.stanford.edu/ jos/pasp/Positive_Real_Functions.html

NN, Dissipative system http://en.wikipedia.org/wiki/Dissipative_system

Appendix

A Definitions

The vector $\mathbf{s}$ is defined a vector of powers of the Laplace operator s. For $s \triangleq j\omega$ and $\omega = 1$ we get the matrices $\mathbf{U}_v$ and $\mathbf{U}_y$, which are needed for determining the signs of polynomials partly replaced by their complex conjugate

$$\mathbf{s} \triangleq (1 \quad s \quad s^2 \quad \ldots)^T \qquad\qquad \mathbf{U}_v \triangleq \mathbf{s}|_{s=j}\mathbf{s}|_{s=j}^H \ , \tag{74}$$

where ^{H} means Hermite, i.e., transposition and the complex conjugate, and * is the complex conjugate without transposition. For the fourth dimension $n = 4$ and $\omega = 1$, one has

$$\mathbf{s}|_{s=j} = \begin{pmatrix} 1 \\ j \\ -1 \\ -j \end{pmatrix}, \qquad \mathbf{U}_v \triangleq \begin{pmatrix} 1 \\ j \\ -1 \\ -j \end{pmatrix} (1 \quad -j \quad -1 \quad j) = \begin{pmatrix} 1 & -j & -1 & j \\ j & 1 & -j & -1 \\ -1 & j & 1 & -j \\ -j & -1 & j & 1 \end{pmatrix} . \tag{75}$$

Correspondingly, one has

$$\mathbf{U}_y \triangleq \mathbf{s}|_{s=j}\mathbf{s}|_{s=j}^T = \begin{pmatrix} 1 & j & -1 & -j \\ j & -1 & -j & 1 \\ -1 & -j & 1 & j \\ -j & 1 & j & -1 \end{pmatrix} . \tag{76}$$

Multiplying two polynomials $a(s)$ and $b^\star(s)$ given by their polynomial coefficients $\mathbf{a}$ and $\mathbf{b}$, respectively, requires the Hadamard product (dot product) and summing up elements in some secondary diagonal referring to Eqs.(16) and (17)

$$(\mathbf{a}\mathbf{b}^T) \ .* \ \mathbf{U}_v \ . \tag{77}$$

The dot product assigns the appropriate sign and imaginary unit j.

A numerical example in MATLAB illustrates the simple results since they can easily lead to some confusion.

```
n=4;   s=[1; j ; -1; -j]; a=[1 2 3 4]';    b=[5 6 7 8]';
Uv=s*s';   Uy= s*conj(s') % (the expression for  s * s^T)
                                  5
                                  4j
                                -10
V1=conv(a .* s, b .* conj(s)) =  - 8j
                                -19
                                  4j
                                 32

                5    - 6j     -7      8j
V2=a*b'.* Uv=  10j    12     -14j   -16
              -15     18j     21    -24j
              -20j   -24      28j    32

Y11=conv([1  2*j -3 -4*j],[5  6*j -7 -8*j]) transposed is equal to

                       5
                      16j
                     -34
Y1=conv(a.*s, b.*s)=  -60j
                      61
                     +52j
                     -32

                  5      6j     -7     -8j
Y2=a*b'.* Uy=   +10j    -12     -14j    16
                -15     -18j     21     24j
                -20j     24     +28j   -32
```

Comparison of $\mathbf{U}_v \triangleq \mathbf{s}|_{s=j}\mathbf{s}|_{s=j}^{H}$ and $\mathbf{U}_y \triangleq \mathbf{s}|_{s=j}\mathbf{s}|_{s=j}^{T}$, Eq.(74) and Eq.(76), offers the only and simple difference in complex conjugation in horizontal direction. Hence, 1 and j are equally distributed. Only each second column differs in sign. Using MATLAB `hintonw` to illustrate the signs, only, one finds Fig. 16 for $n = 9$. For $n = 5,\ 9,\ 13, \ldots$ etc., $\mathbf{U}_v$ and $\mathbf{U}_y$ are reflected by a vertical axis as far as the signs only are concerned.

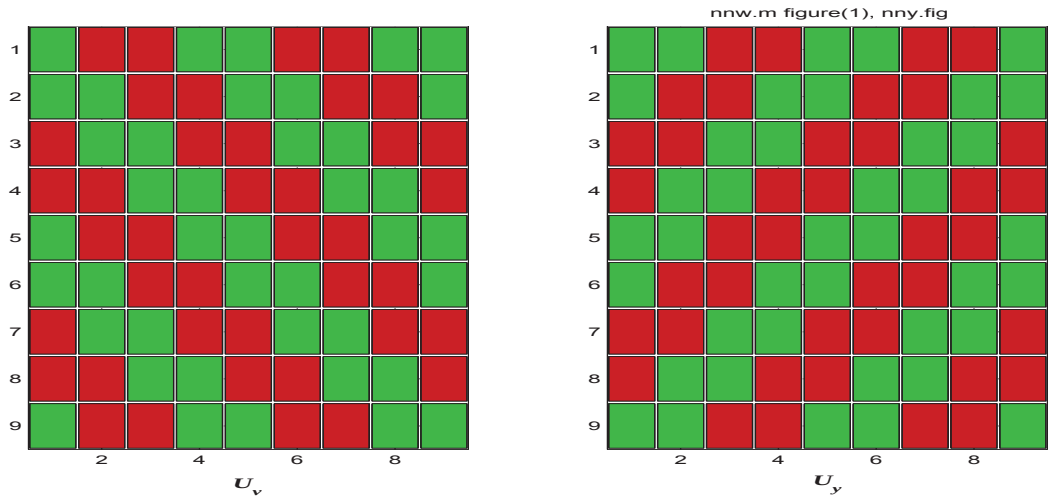

Figure 16: Sign pattern of $\mathbf{U}_v$ and $\mathbf{U}_y$ for $n = 9$

To continue, define the reduced unity matrix

$$\mathbf{I}_{i\times n} \stackrel{\triangle}{=} \text{e.g.,}\mathbf{I}_{2\times 4} = \begin{pmatrix} 1 & 0 & 0 & 0 \\ 0 & 1 & 0 & 0 \end{pmatrix} , \tag{78}$$

which corresponds to the unity matrix $\mathbf{I}_n$ with deleted rows higher than i.

The reflection matrix $\mathbf{I}_R$ reads as

$$\mathbf{I}_R \equiv \mathbf{I}^{\swarrow} = \mathbf{I}_{Rn} \stackrel{\triangle}{=} \begin{pmatrix} 0 & 0 & 1 \\ 0 & 1 & 0 \\ 1 & 0 & 0 \end{pmatrix} \quad \text{for} \quad n = 3. \tag{79}$$

Premultiplying a matrix with the reflection matrix yields the matrix which is reflected with respect to a horizontal line; postmultiplying results in a reflection along a vertical line.

B Positive Definiteness

The main (leading) principal minors d_i of the matrix $\mathbf{Q} \in \mathcal{R}^{n\times n}$ (where only symmetric matrices make sense in square functions $\mathbf{x}^T\mathbf{Q}\mathbf{x}$) are

$$d_i \stackrel{\triangle}{=} \det \begin{pmatrix} Q_{11} & \dots & Q_{11} \\ \vdots & \ddots & \vdots \\ Q_{i1} & \dots & Q_{ii} \end{pmatrix} , \quad 1 \le i \le n , \quad Q_{i1} = Q_{1i} , \tag{80}$$

$d_n = \det \mathbf{Q}$. For $\mathbf{Q} = \mathbf{Q}^T$ all $\lambda[\mathbf{A}]$ are real and $\mathbf{Q} > 0$. $\mathbf{Q}$ is positive definite, i.e., $\mathbf{x}^T\mathbf{Q}\mathbf{x} > 0$, $\forall \mathbf{x} \neq \mathbf{0}$, iff $d_i > 0 \quad \forall 1 < i < n$.

C Review of Lyapunov Stability Properties for Linear Systems

We recall some important properties for linear systems Lyapunov theory. Assuming an autonomous system $\dot{\mathbf{x}} = \mathbf{A}\mathbf{x}$ with $\mathbf{A} \in \mathcal{R}^{n\times n}$, and defining a Lyapunov function

$$V = V(\mathbf{x}) = \mathbf{x}^T\mathbf{P}\mathbf{x} \ , \tag{81}$$

the derivative with respect to time is

$$\dot{V}(\mathbf{x}) = \mathbf{x}^T(\mathbf{A}^T\mathbf{P} + \mathbf{P}\mathbf{A})\mathbf{x} \stackrel{\triangle}{=} -\mathbf{x}^T\mathbf{Q}\mathbf{x} \ , \tag{82}$$

where the algebraic Lyapunov equation is

$$\mathbf{A}^T\mathbf{P} + \mathbf{P}\mathbf{A} + \mathbf{Q} = \mathbf{0} \ . \tag{83}$$

Both $\mathbf{P}$ and $\mathbf{Q}$ being positive definite symmetric is a necessary and sufficient condition for $\mathbf{A}$ stable (*Kalman, R.E., and Bertram, J.E., 1960; Slotine, J.J., and Weiping, Li, 1991,* Remember:

- Irrespective weather $\mathbf{P}$ is selected and $\mathbf{Q}$ is found from Eq.(83), the system is stable if both are positive definite.

- If one of the matrices $\mathbf{P}$ and $\mathbf{Q}$ fails positive definiteness it depends on the initial assumption. Choosing $\mathbf{Q} > 0$ and computing $\mathbf{P} < 0$, the system is unstable due to the following facts: If $\mathbf{A}$ has eigenvalues throughout with negative real parts and $\mathbf{Q}$ is positive definite then $\mathbf{Q}$ can be written as $\mathbf{Q} = \mathbf{M}^T\mathbf{M}$

$$\mathbf{P} \stackrel{(88),(89)}{=} \int_0^\infty e^{\mathbf{A}^T\tau}\ \mathbf{M}^T\mathbf{M}\ e^{\mathbf{A}\ \tau}\ d\tau \tag{84}$$

$$\mathbf{x}^T\mathbf{P}\mathbf{x} = \int_0^\infty \mathbf{x}^T\ e^{\mathbf{A}^T\tau}\ \mathbf{M}^T\mathbf{M}\ e^{\mathbf{A}\ \tau}\ \mathbf{x}\ d\tau = \int_0^\infty \ \parallel \mathbf{M}\ e^{\mathbf{A}\ \tau}\ \mathbf{x}\ \parallel_F^2\ d\tau \geq 0 \ . \tag{85}$$

- If $\mathbf{P}$ is selected first and Eq.(83) yields a negative definite $\mathbf{Q}$, no result can be deduced. Even for stable $\mathbf{A}$ and positive definite $\mathbf{P}$, $\mathbf{Q}$ may turn out negative definite, because Eq.(85) is not satisfied, see, e.g., *Slotine, J.J.,* for an example of such an inconclusive result.

- An optimum lower and upper bound of the convergence rate in the relation $\dot{V}/V$ and $V[\mathbf{x}(t)]$ can be given as by simply selecting $\mathbf{Q} = \mathbf{I}$, following from

$$-\frac{\lambda_{\max}[\mathbf{Q}]}{\lambda_{\min}[\mathbf{P}]} \ \leq\ \frac{\dot{V}(\mathbf{x})}{V(\mathbf{x})} = -\frac{\mathbf{x}^T\mathbf{Q}\mathbf{x}}{\mathbf{x}^T\mathbf{P}\mathbf{x}} = -\frac{\mathbf{x}^T\mathbf{Q}\mathbf{x}/\mathbf{x}^T\mathbf{x}}{\mathbf{x}^T\mathbf{P}\mathbf{x}/\mathbf{x}^T\mathbf{x}} \ \leq -\frac{\lambda_{\min}[\mathbf{Q}]}{\lambda_{\max}[\mathbf{P}]} \tag{86}$$

$$\exp\ \{-\frac{1}{\lambda_{\min}[\mathbf{P}]}t\} \ \leq\ \frac{V[\mathbf{x}(t)]}{V[\mathbf{x}_o]} \ \leq \exp\ \{-\frac{1}{\lambda_{\max}[\mathbf{P}]}t\} \ . \tag{87}$$

- Consider the Lyapunov matrix equation as the special case $t \to \infty$ of the linear matrix differential equation with free upper integral limit t,

$$\dot{\mathbf{P}}(t) = \mathbf{A}^T\mathbf{P}(t) + \mathbf{P}(t)\mathbf{A} + \mathbf{Q} \qquad \text{where} \qquad \mathbf{P}(0) = \mathbf{0} \ , \tag{88}$$

the result is is given by

$$\mathbf{P}(t) = \int_0^t e^{\mathbf{A}^T\tau} \ \mathbf{Q} \ e^{\mathbf{A} \ \tau} \ d\tau \ . \tag{89}$$

For $\mathbf{P}(t) \to 0$ as $t \to \infty$, Eq.(88) approaches Eq.(83). Hence, the solution of the algebraic Lyapunov equation Eq.(83) is given by Eq.(84).

For Lyapunov theoretical aspects, based on and derived from Linear Matrix Inequalities, see *Ostertag, E., 2010.*

D Failures to Positive Realness Conditions

Further examples for objecting the positive realness conditions are given in Figs. (17) and (18). The line $a = c - b$ is the borderline.

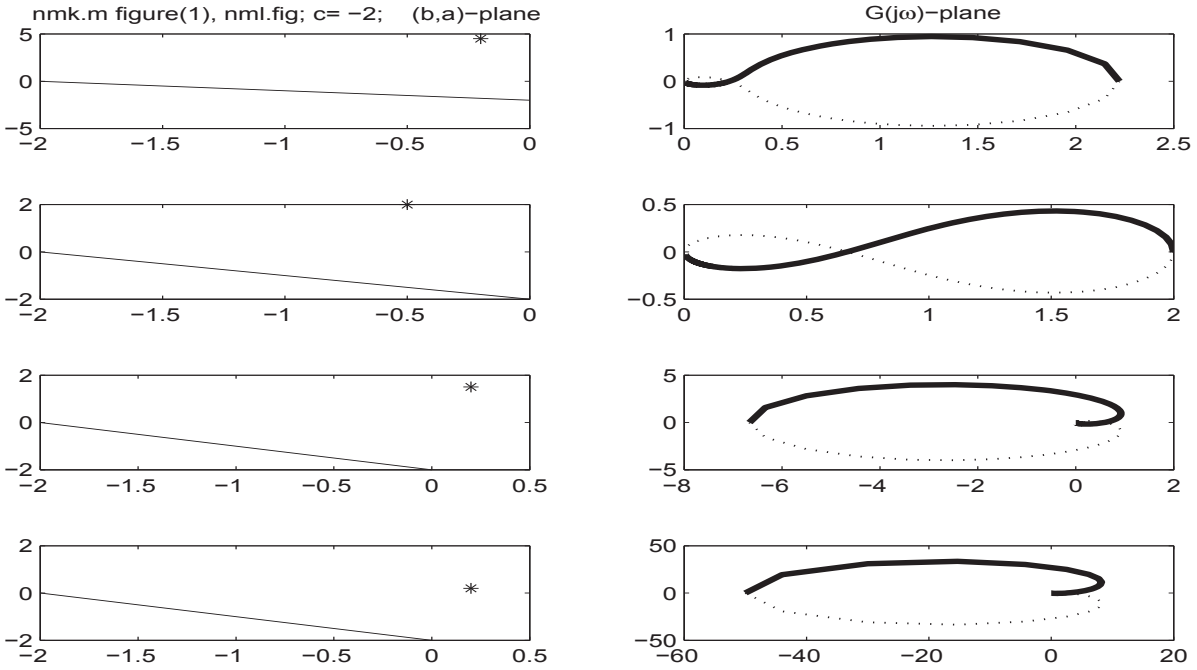

Figure 17: Examples objecting positive realness for $c = -2$ (Illustration 1)

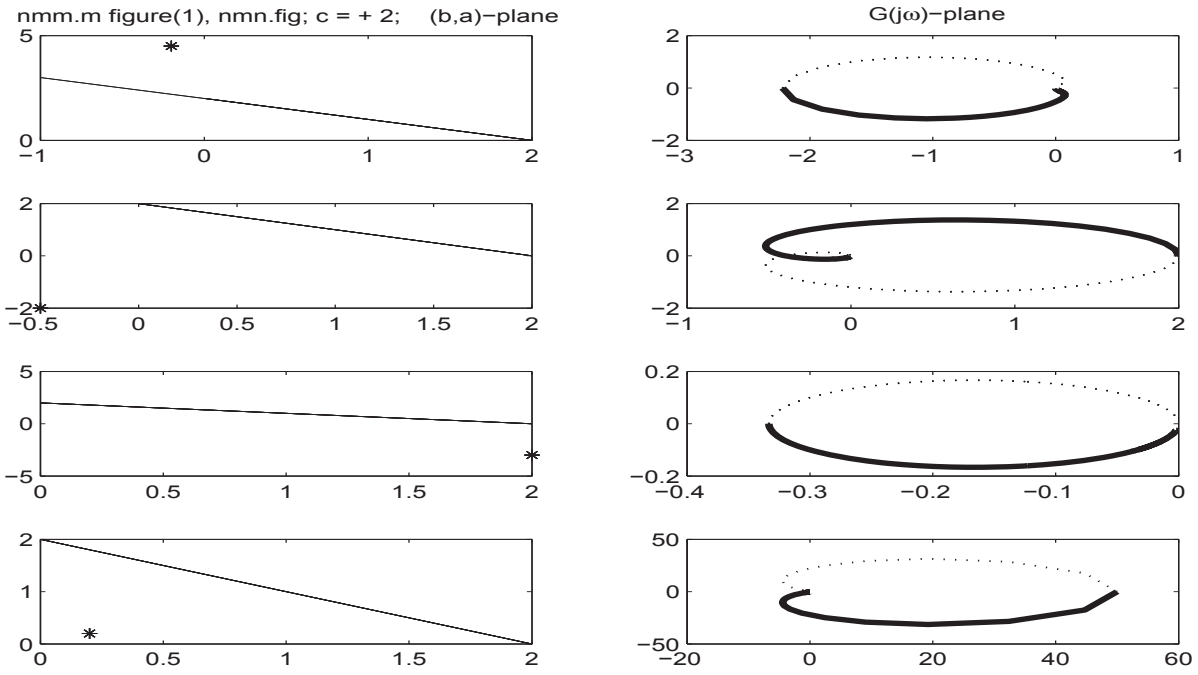

Figure 18: Some more examples objecting positive realness for $c = +2$ (Illustration 1)

Der 25. Österreichische Automatisierungstag an der Alpen-Adria Universität Klagenfurt

Der Österreichische Automatisierungstag 2010 war dieses Jahr den zukunftsträchtigen Themen „Energie und Mobilität“ gewidmet. Austragungsort war erstmals die Alpen-Adria Universität Klagenfurt, an der im Jahre 2007 die Fakultät für technische Wissenschaften gegründet wurde. Organisiert wurde die Jubiläumsveranstaltung von Professor Martin Horn vom Lehrstuhl für Mess- und Regelungssysteme der Universität Klagenfurt. Das Vortragsprogramm umfasste Vorträge von Vertretern aus Industrie und Forschung und gab einen Überblick über aktuelle und zukünftige Entwicklungen im Bereich der Verkehrs- und Energiesysteme.

Professor Wolfgang Hirschberg vom Institut für Fahrzeugtechnik der Technischen Universität Graz gab in seinem Vortrag *„E-Mobility - Diversifizierung oder Allround-Kfz?“* einen Überblick über zukunftsträchtige Antriebssysteme für straßengebundene Kraftfahrzeuge. Anhand aktueller Statistiken verdeutlichte er, dass die meisten Fahrten auch heute schon problemlos mit Elektrofahrzeugen bewältigt werden könnten. Verbesserungspotentiale sieht Professor Hirschberg vor allem in der Entwicklung von leistungsfähigeren Energiespeichersystemen. Genau zu dieser Thematik passend berichtete Dr. Stefan Doczy von der „Magna E-Car Systems GmbH“ in seinem Vortrag „*Entwicklung und Test von Batteriesystemen für Nutzfahrzeuge*“ über aktuelle Entwicklungen im Bereich der Batteriesysteme im Nutzfahrzeugbereich. Dr. Doczy widmete sich vor allem der Planung und Durchführung der aufwändigen Testprozeduren für Batteriesysteme, denen im Entwicklungsprozess eine besondere Bedeutung zukommt.

Professor Kyandoghere Kyamakya vom Lehrstuhl für Verkehrsinformatik der Alpen-Adria Universität Klagenfurt stellte in seinem Vortrag „*Eine Extended Floating Car Data Infrastruktur zur Unterstützung der Fahrerassistenz hinsichtlich Echtzeit-Fahrsicherheit sowie Eco-Driving*“ ein in Entwicklung befindliches Fahrassistenzsystem vor, das durch Nutzung multipler Informationsquellen die Sicherheit des Straßenverkehrs in Zukunft signifikant verbessern soll.

Von der Straße auf die Schiene wechselte Dr. Martin Rosenberger von der „vif - Das virtuelle Fahrzeug GmbH“, der die „*Potentiale von mechatronischen Systemen in der Schienenfahrzeugtechnik***“** aufzeigte. Trotz konservativer und daher träger Strukturen im Bahnwesen setzen sich auch dort moderne mechatronische Systeme durch, die nicht nur den Fahrkomfort verbessern, sondern durch Verschleißminimierung auch die Lebensdauer von Schienenfahrzeugen erheblich verlängern können.

Dipl.-Ing. Rene Jilg skizzierte in seinem Vortrag „*Windkraftanlagen gestern und heute Herausforderungen an die moderne Technik*“ die technischen Fortschritte bei der

Entwicklung von Windkraftanlagen. Anhand eindrucksvoller Animationen veranschaulichte er die regelungstechnischen Herausforderungen bei der Beherrschung der immer größer werdenden Windanlagen.

Mathematische Modelle und darauf aufbauende Regelalgorithmen für Biomassefeueranlagen präsentierte Dr. Markus Gölles von der „BIOENERGY 2020+ GmbH“ in seinem Vortrag mit dem Titel „*Effizientere Biomassefeuerungsanlagen durch modellbasierte Regelungsstrategien*“. Die vorgestellten Ansätze wurden ausführlich erläutert, ihre praktische Tauglichkeit wurde anhand von Messergebnissen, die an einer realen Versuchsanlage gewonnen wurden, eindrucksvoll demonstriert.

Ein fester Bestandteil und Höhepunkt des Österreichischen Automatisierungstages ist traditionell die Verleihung des Fred Margulies Preises durch Dr. Norbert Rozsenich und Professor Peter Kopacek. Dieses Jahr wurden sechs Preisträger geehrt, und zwar Herr Dipl.-Ing. Markus Egretzberger für seine Arbeit mit dem Titel „Mathematical Modeling and Control of Electromechanical Gyroscopes“, Herr Dipl.-Ing. Werner Mastny für seine Arbeit mit dem Titel „Improvement of the mechanical construction of advanced mobile robots for Landmine detection“; Herr Dipl.-Ing. Dr. Mario Richtsfeld für seine Arbeit mit dem Titel „Robust Range Image Processing for Robot Manipulation“, Herr Dipl.-Ing. Richard Stadlmayr für seine Arbeit mit dem Titel „On a Combination of Feedforward and Feedback Control for Mechatronic Systems“, Herr Dipl.-Ing. Hannes Trogmann für seine Arbeit mit dem Titel „Neue Regelverfahren für eine pneumatische Stewart Plattform“ und Herr Dr. Alois Zoitl für seine Arbeit mit dem Titel „Basic Real-Time Reconfiguration Services for Zero Down-Time Automation Systems“

Zusammenfassend kann der Automatisierungstag 2010 als sehr gelungen bezeichnet werden. Dies spiegelt sich auch im großen Interesse des Publikums wider - mehr als 60 ZuhörerInnen verharrten bis zum Ende der Veranstaltung.

Univ. Prof. Martin Horn
Lehrstuhl für Mess- und Regelungssysteme
Alpen-Adria Universität Klagenfurt

Greifertechnik
Effektoren für Roboter und Automaten

Stefan Hesse

ISBN 978-3-446-42422-7

Carl Hanser Verlag, München 2011

Die Erweiterung der Anwendungsgebiete von Robotern, Manipulatoren und Handhabungseinrichtungen erfordert immer mehr flexible und leistungsfähige Greifer. Greifen ist eine Grundbewegung in der Robotertechnik zum Erfassen und Halten von Objekten. Durch Greifen wird eine zeitweilige Verbindung zwischen Roboter und Werkstück hergestellt. Aufbau, Funktion und Einsatz von Greifern (Effektoren, Endeffektor) gehören zum Kernwissen in der Automation von Handhabungs- und Montagevorgängen. Besonders in diesem Bereich strebt man nach Flexibilität, Automation und Höchstleistung. Davon sind in hohem Maße die Greifeinrichtungen betroffen und nehmen eine Schlüsselstellung ein.

Im Buch werden die Grundlagen systematisch dargestellt: die wirkenden physikalischen Prinzipien, die Bandbreite der wichtigsten Bauformen, die Berechnung von Greifern, Kinematik, sensorische Ausstattungen sowie typische Anwendungsfälle und Sonderlösungen. Die für industrielles Greifen benötigten Greifer werden in diesem Buch vorgestellt und sind in vielen Ausführungen erhältlich. Eigenschaften und Anforderungsbild sind entscheidend für die Auswahl eines Greifersystems und die Gestaltung der Greiforgane.

Mit vielen Lösungsanregungen und über hundert Konstruktionszeichnungen von Greifern enthält das Buch auch direkt in der Praxis verwendbares Wissen und wendet sich an Techniker, Konstrukteure, Ingenieure und auch an Studenten maschinenbaulicher Studienrichtungen.

Peter Kopacek

Zukunft der Produktion
Herausforderungen, Forschungsfelder, Chancen

E. Abele, G. Reinhart

Carl Hanser Verlag , 2011
ISBN 978-3-446-42595-8

Der Produktionsstandort Deutschland kann sich im globalen Wettbewerb nur behaupten, wenn die Unternehmen auf die zukünftigen Anforderungen eingestellt sind. Das vorliegende Buch zeigt ausgehend von den Megatrends, welche Aktionsfelder die Produktionsforschung in den nächsten zehn Jahren bearbeiten muss, um vorne zu sein. Sei es der demografische Wandel, neue Technologien, Klimawandel, Ressourcenknappheit oder Mobilität; jeder dieser Einflussfaktoren verlangt gezielte Anpassungen in der Produktion und im Unternehmen. Es wird beschrieben, wie diese aussehen sollten: neue Produkte und Märkte, Paradigmenwechsel in Organisation und Management, neue Fertigungstechnologien, nachhaltige Prozesse. Auf jede Herausforderung gibt es Antworten und Handlungsempfehlungen. Ein wertvolles Buch für Führungskräfte, die Zukunft mit gestalten.

Das vorliegende Buch beginnt mit einem „Management Summary“ in dem eine übersichtliche Darstellung der sieben Kapiteln in Form von Abstracts erfolgt. Sodann werden die Herausforderungen an die Produktion der Zukunft dargestellt sowie ein Leitbild dafür erstellt. Die nächsten Kapitel widmen sich den Forschungsthemen zur Umsetzung dieses Leitbildes sowie dazu erforderliche Forschungsthemen. Zum Abschluss wird die integrative Rolle der Produktion und die Zusammenarbeit zwischen Industrie und Wissenschaft anhand von erfolgreichen Verbundprojekten dargestellt.

Das Buch kann sowohl in der Praxis stehenden als auch wissenschaftlich tätigen Ingenieuren und Managern, überwiegend in Deutschland, empfohlen werden.

P. Kopacek

Instruction to authors – presented as a pattern paper (18 pt)

A. Maier, F. Huber (12 pt)
Department ....., Vienna, Austria

Received April 8, 1999

Abstract
This paper shows …… (italics, 12 pt)

1 General (14 pt)

Authors should prepare their manuscript camera ready, format A 4, 12 typeface and must present their manuscript in good quality. At the left/right edge 2.5 cm, at the to/bottom edge 3 cm. Authors are invited to use papers of this journal as a sample. Please do not use an eraser or erasing fluid. Footnotes should be avoided if possible. Authors are expected to submit their paper to one of the publishers (O.Univ.Prof.Dr. Peter Kopacek, Intelligent Handling Devices and Robotics, Vienna University of Technology, Favoritenstrasse 9-11, A-1040 Vienna, Austria, Fax: +43 1 58801-31899 or O.Univ.Prof.Dr. Alexander Weinmann, Institute of Automation and Control, Vienna University of Technology, Gusshausstr. 27-29, A-1040 Vienna, Austria, Fax: +43 1 58801 37699).

Email address for submitting pdf-manuscripts: weinmann@acin.tuwien.ac.at

2 References (14 pt)

Within the paper references should appear in the following form:
(Mayer, H., 1990) or (*Mayer, H., 1990)* (12 pt);
Mayer, H., 1990, discovered that....

3 Figures and Tables (14 pt)

Figures and Tables should be integrated in the paper and have to be referred to as Fig. 4.1 or Tab. 5.2.

4 References

References are to be listed alphabetically according to first author. (11 pt)

5 Word Processing System/Editor

Microsoft Word 2000 or higher; TeX or LaTeX.

Wenn unzustellbar, retour an:

IFAC-Beirat Österreich (E318 / E376)
Favoritenstraße 9-11, A-1040 Wien /
Gußhausstraße 27-29, A-1040 Wien